

A chronology of early Mars climatic evolution from impact crater degradation

N. Mangold, S. Adeli, Susan J. Conway, V. Ansan, B. Langlais

▶ **To cite this version:**

N. Mangold, S. Adeli, Susan J. Conway, V. Ansan, B. Langlais. A chronology of early Mars climatic evolution from impact crater degradation. Journal of Geophysical Research. Planets, 2012, 117 (E4), pp.n/a-n/a. 10.1029/2011JE004005 . insu-02276068

HAL Id: insu-02276068

https://insu.hal.science/insu-02276068

Submitted on 5 Mar 2021

HAL is a multi-disciplinary open access archive for the deposit and dissemination of scientific research documents, whether they are published or not. The documents may come from teaching and research institutions in France or abroad, or from public or private research centers.

L'archive ouverte pluridisciplinaire **HAL**, est destinée au dépôt et à la diffusion de documents scientifiques de niveau recherche, publiés ou non, émanant des établissements d'enseignement et de recherche français ou étrangers, des laboratoires publics ou privés.

A chronology of early Mars climatic evolution from impact crater degradation

N. Mangold,[1] S. Adeli,[1,2] S. Conway,[1] V. Ansan,[1] and B. Langlais[1]

Received 13 October 2011; revised 9 January 2012; accepted 18 February 2012; published 12 April 2012.

[1] The degradation of impact craters provides a powerful tool to analyze surface processes in the Martian past. Previous studies concluded that large impact craters (20–200 km in diameter) were strongly degraded by fluvial erosion during early Martian history. Our goal is to study the progression of crater degradation through time with a particular emphasis on the craters with alluvial fans and on the relative chronology of these craters. The geometric properties of 283 craters of >20 km in diameter were analyzed in two highlands of Mars, north of Hellas Planitia, and south of Margaritifer Terra, both known to contain craters with alluvial fans. Three classes were defined from morphology: strongly degraded craters with fluvial landforms and without ejecta (type I), gently degraded craters with fluvial landforms and preserved ejecta (type II), and fresh craters with ejecta and no fluvial landforms (type III). Our main result is that the type II craters that present alluvial fans have characteristics closer to fresh craters (type III) than degraded craters (type I). The distinctive degradation characteristics of these classes allowed us to determine a temporal distribution: Type I craters were formed and degraded between ~4 Gyr and ~3.7 Gyr and type II craters with alluvial fans were formed between Early Hesperian and Early Amazonian (~3.7 to ~3.3 Gyr). This chronology is corroborated by crosscutting relationships of individual type II craters, which postdate Late Noachian valley networks. The sharp transition at ~3.7 Gyr suggests a quick change in climatic conditions that could correspond to the cessation of the dynamo.

Citation: Mangold, N., S. Adeli, S. Conway, V. Ansan, and B. Langlais (2012), A chronology of early Mars climatic evolution from impact crater degradation, *J. Geophys. Res.*, *117*, E04003, doi:10.1029/2011JE004005.

1. Introduction

[2] Impact crater degradation provides a powerful tool to analyze past Martian climate. Previous studies concluded that large impact craters were strongly degraded during early Martian history (<3 Gyr), whereas younger craters are only weakly degraded [*Craddock and Maxwell*, 1990; *Craddock et al.*, 1997]. Based on Viking data, this ancient degradation was attributed to fluvial erosion, because no other process (i.e., eolian or glacial activity, volcanism) could adequately reproduce the topographic profiles of degraded craters [*Craddock et al.*, 1997]. Specifically, craters with no or low rims must have been modified by erosion, and not by an aggradational process such as volcanic or aeolian filling [*Craddock and Maxwell*, 1990; *Craddock and Maxwell*, 1993]. *Forsberg-Taylor et al.* [2004] performed numerical simulations of crater degradation by fluvial and eolian process and they also concluded that fluvial erosion was most consistent with the observed topography. Degraded craters are therefore one of the main lines of evidence for a warmer climate on early Mars. Other lines of evidence include, the extensive identification of phyllosilicates in the Noachian crust [e.g., *Poulet et al.*, 2005; *Bibring et al.*, 2006; *Loizeau et al.*, 2007; *Mangold et al.*, 2007; *Mustard et al.*, 2009; *Dehouck et al.*, 2010] and fluvial valley networks [e.g., *Carr*, 1996; *Craddock and Howard*, 2002; *Howard et al.*, 2005; *Irwin et al.*, 2005; *Ansan and Mangold*, 2006; *Fassett and Head*, 2008, 2011].

[3] Initial studies of crater degradation were conducted using Viking images morphologic interpretation and topography from photoclinometric profiles, i.e., using radiometric variation in Viking images [*Craddock et al.*, 1997]. Global altimetry and recent high-resolution imagery enable us to revisit this work with much better data sets. These data allowed us to pick out fine details in the morphology of degraded craters. In particular it allowed us to identify preserved impact ejecta, which is strong evidence for limited degradation, and fluvial landforms on rims. These details were particularly pertinent in the case of the craters with alluvial fans [*Moore and Howard*, 2005]. Indeed, post-Viking imagery showed the presence of alluvial fans in some of these ancient craters, which are clear signatures of enhanced fluvial erosion and deposition in craters without

[1]Laboratoire Planétologie et Géodynamique de Nantes, LPGN/CNRS UMR6112 and Université de Nantes, Nantes, France.
[2]Now at DLR Institute of Planetary Research, Berlin, Germany.

Copyright 2012 by the American Geophysical Union.
0148-0227/12/2011JE004005

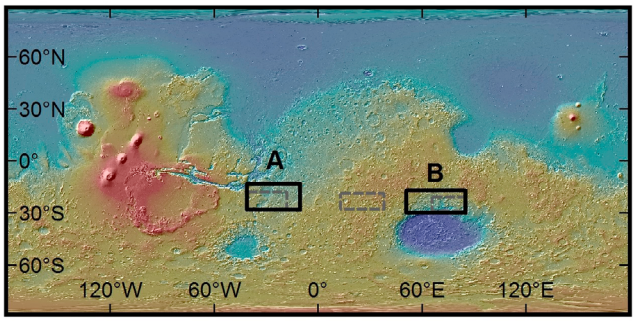


Figure 1. MOLA topography superimposed on MOLA hill shade with our study regions marked: box A is southern Margaritifer Terra (SMT) and box B is north Hellas Planitia (NHP), and dotted gray boxes are those areas studied by *Moore and Howard* [2005].

standing bodies of water [*Moore and Howard*, 2005, *Kraal et al.*, 2008]. Fans in these craters were interpreted as being due to a climatic optimum, at the Noachian-Hesperian transition. As a consequence, we chose to focus our study on the craters with alluvial fans; their degradation stage, the type of fluvial erosion, and on their chronology relative to other climatic markers such as the global valley networks.

[4] After having first presented the data sets, methods and regions studied, we present a qualitative classification of the morphology of the impact craters studied using simple parameters such as the presence of fluvial erosion and of impact ejecta. Then, a quantitative analysis of these crater classes is presented to link the morphometric degradation with the geometric modification and tie it in to the chronology of Mars. Last, the results are discussed in broader context with particular focus on Mars' climatic evolution.

2. Approach and Methods

2.1. Study Regions

[5] Our study focused on two large areas of the Noachian highlands where alluvial fans in craters were found by *Moore and Howard* [2005]: Northern Hellas Planitia (NHP) at −17°S to −30°S latitude and 51°E to 85°E longitude and Southern Margaritifer Terra (SMT) at 13°S to 28°S latitude and 320°W to 350°W longitude (Figure 1). These two regions are slightly larger than those initially studied by *Moore and Howard* [2005], because we found more craters with alluvial fans in these surrounding areas, some of them having been noted by *Kraal et al.* [2008] as well. The crater properties were extracted for a total of 283 impact craters of >20 km in diameter in the two studied areas, a number providing better confidence in the statistics.

[6] The NHP study site consists almost exclusively of Noachian highlands terrain including extensive valley networks, both SE of Huygens crater [*Ansan et al.*, 2008] and in the southern Tyrrhena region [*Mest et al.*, 2010]. There is widespread sedimentary in-filling toward Hellas Planitia, for example, the Terby impact crater [*Wilson et al.*, 2007] where the 2 km thick deposits have been interpreted to be of deltaic origin [*Ansan et al.*, 2011]. This region has craters that range from fresh to strongly degraded all of which postdate the Hellas basin, because they are all superposed on its northern rim.

[7] The SMT study site is composed of Noachian highlands with local intercrater plains such as in Ladon basin. This region is less homogeneous than NHP in geological context, with tectonic features related to the SE margin of Tharsis, chaotic terrains and outflow channels. Well-developed valley networks are present mainly to the east of the area, e.g., Loire Vallis and Samara Vallis, but valleys also exist in the western area, sometimes with depositional fans, for example, in and around Holden and Eberswalde craters [*Grant et al.*, 2008; *Malin and Edgett*, 2003; *Pondrelli et al.*, 2008]. The SMT region has a few craters which contain large polygonal blocks, resembling chaos terrain, which probably correspond to degradation related to subsurface processes rather than climatic ones [e.g., *Chapman and Tanaka*, 2002, *Rodriguez et al.*, 2005, *Meresse et al.*, 2008]. Nevertheless, ancient terrains predominate the area, which offers a good statistical set of >20 km diameter craters.

2.2. Data Sets and Methods

[8] The High Resolution Stereo Camera (HRSC) instrument acquires images in five panchromatic channels under different observation angles, as well as four color channels at a relatively high spatial resolution [*Neukum and Jaumann*, 2004]. In this work we used only panchromatic nadir images, with a maximum spatial scale from 10 to 40 m/pixel. CTX images (Context Camera [*Malin et al.*, 2007]) were used to determine the detailed morphology of features within the two study areas, especially identification of ejecta and fluvial erosion. A few High Resolution Imaging System (HiRISE) images at 25 cm/pixel were used to focus on the fine detail of some impact craters [*McEwen et al.*, 2007]. Thermal Emission Imaging System (THEMIS) images [*Christensen et al.*, 2003] with a resolution of ∼100 m/pixel were used to complement visible imagery, especially when the thermal properties display variations consistent with distinct geomorphic landforms, such as ejecta blankets.

[9] Mars Orbiter Laser Altimeter (MOLA) gridded data at ∼463 m/pixel [*Smith et al.*, 1999] were used to extract topographic information for the surveyed craters. While this data set contains artifacts at full resolution, the use of craters >20 km limits these effects. To avoid errors caused by the distortion of a regional map projection, each crater was projected into a local sinusoidal projection, with the central meridian of the projection being the same as the longitude of the crater's center. The rim of each crater was digitized as a circle using the HRSC and CTX images and a slope map derived from MOLA data. The crater's center point and radius were estimated from these circles. The distance and angular displacement from the center point was calculated for every pixel up to 1.5 crater radii from the center point. Each crater was divided into eight 10° wide segments, facing the cardinal directions, north, NE, east, etc. (Figure 2). The width of the segments, was therefore always >3.4 km at the rim, thus includes both interpolated and noninterpolated pixels. For each of these segments a radial elevation profile was constructed by averaging the MOLA elevation pixels within each concentric 500 m distance bin. Central peaks were ignored in the calculation; the base of the crater was taken as the lowest point. For each profile the following were calculated: crater depth, radius, inner rim maximum

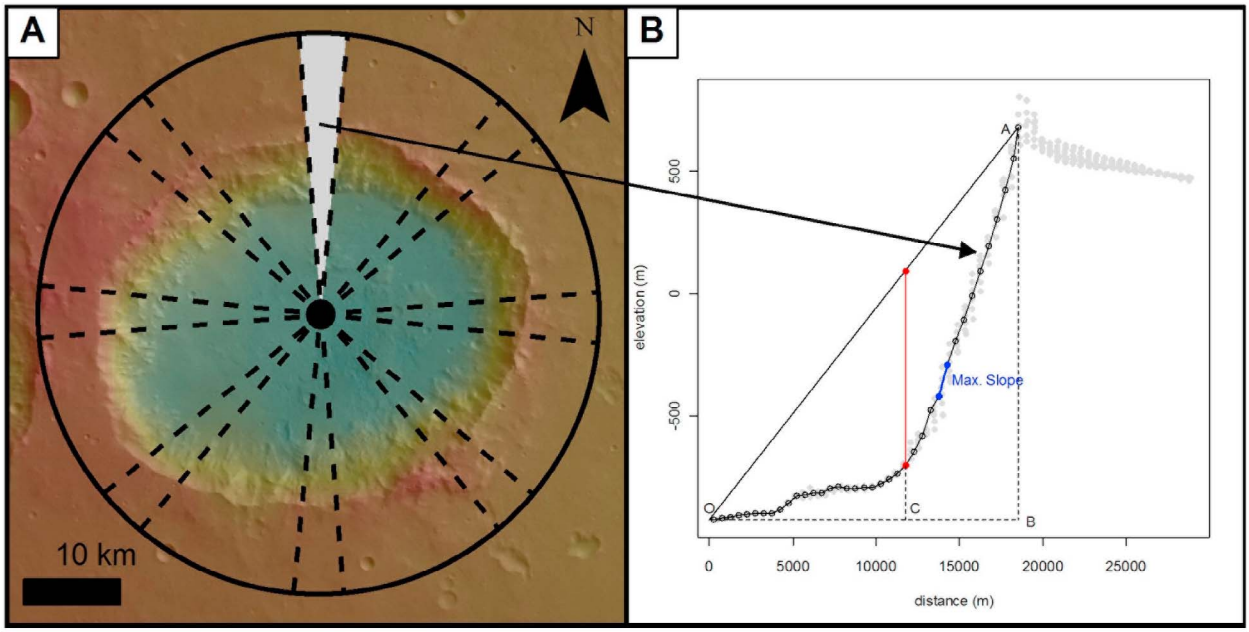


Figure 2. Illustration of method to extract geometric properties for craters. (a) Black dot is the crater center, and solid line is a circle at 1.5 crater radii. Dotted lines delimit 10° zones oriented north, NE, east, SE, south, SW, west and NW. Data from the south facing segment (highlighted), is shown in Figure 2b. HRSC image H0533_0000 overlain on MOLA topography in color. (b) An example profile with gray dots being the raw MOLA data and black circles showing the calculated mean profile connected with lines. The profile section used for the slope calculation is indicated. The curvature is given by the ratio of OC to OB. OC is the distance to the basal concavity. This is calculated by finding the position of the maximum difference between the line OA and each point in the profile (here highlighted by the solid vertical line).

slope and inner rim curvature, and the mean of the eight segments was taken as representative of the crater as a whole. We calculated the standard deviation of each parameter for the eight profiles to assess the variability for each crater (Tables 1 and 2). The crater radius was used to determine the crater's diameter and therefore its depth-diameter ratio. The inner rim curvature was quantified by measuring the relative distance to the basal concavity (Figure 2). This was performed by finding the distance at which the difference between the crater profile and the straight line joining the base to the rim of the crater was greatest, i.e., the inflection point. This distance was then normalized by the crater radius. Values near zero correspond to craters that are conical, with straight walls, values near 0.5 to bowl-shaped craters and values near 1 to craters with rectilinear walls, i.e., with a large flat base and steeper walls. The maximum slope was calculated by finding the maximum drop between two adjacent points on the average profile. Hence, because the profile itself is produced from average data, including noise and interpolated pixels this value will be an underestimate of the actual 500 m baseline maximum slope. However, the underestimate is of the same magnitude for all the craters.

3. Geomorphic Analysis and Classification of Impact Crater Degradation

3.1. Identification of Central Peaks and Ejecta

[10] The freshness of craters can be evaluated using two main landforms: central peaks and ejecta. The preservation or burial of central peaks is an important parameter to evaluate

Table 1. Summary of Standard Deviations of the Eight Measurements for Each Crater for Each of the Parameters Measured in Both Study Areas[a]

Type	n	Diameter Normalized	Depth Normalized	Slope (m/m)	Curvature
			North Hellas Planitia		
I	125	0.058 ± 0.002	0.31 ± 0.016	0.423 ± 0.018	0.118 ± 0.006
II	23	0.057 ± 0.003	0.152 ± 0.018	0.297 ± 0.023	0.087 ± 0.007
III	17	0.053 ± 0.005	0.132 ± 0.013	0.257 ± 0.023	0.082 ± 0.008
			Southern Margaritifer Terra		
I	79	0.06 ± 0.002	0.245 ± 0.021	0.442 ± 0.022	0.126 ± 0.008
II	18	0.045 ± 0.004	0.109 ± 0.014	0.248 ± 0.024	0.077 ± 0.006
III	12	0.055 ± 0.005	0.091 ± 0.01	0.249 ± 0.024	0.088 ± 0.008

[a]The mean standard deviation of each parameter is followed by the standard. The depth-diameter and slope have been normalized by the average depth, diameter and slope, respectively.

Table 2. Summary of Physical Attributes Measured for Each Crater Type in Both Study Areas[a]

Type	n	Depth-Diameter	Slope (m/m)	Curvature
		North Hellas Planitia		
I	97	0.036 ± 0.001	0.26 ± 0.01	0.67 ± 0.01
II	10	0.052 ± 0.004	0.39 ± 0.02	0.57 ± 0.01
III	18	0.068 ± 0.002	0.43 ± 0.01	0.56 ± 0.01
		Southern Margaritifer Terra		
I	58	0.03 ± 0.002	0.25 ± 0.01	0.69 ± 0.01
II	10	0.057 ± 0.002	0.41 ± 0.02	0.61 ± 0.01
III	11	0.067 ± 0.004	0.44 ± 0.03	0.6 ± 0.01

[a]Limited to craters <50 km only to avoid bias induced by the lack of type III craters for diameters >50 km. The standard error of each parameter is given after each value. Standard error was chosen rather than standard deviation in order to take into account the different number of craters in each category.

the relative degradation of craters in the size range of 20 to 100 km. Above 100–150 km complex craters often do not have well-developed central peaks, due to collapse and crustal scale relaxation on impact [e.g., *Melosh*, 1989]. Central peaks are sometimes preserved after significant erosion, even on Earth [e.g., *Milton et al.*, 1972], and the infill can be related to volcanic activity rather than sedimentary deposition. So, this parameter is useful, but central peak preservation is not uniquely representative of relatively fresh impact craters.

[11] Impact ejecta, however, are comparatively thin landforms that are usually <200 m thick for impact diameters <100 km [*McGetchin et al.*, 1973; e.g., *Melosh*, 1989]. Their thickness close to the rim corresponds to about 3% of the crater diameter [*Pike*, 1974]. Thin ejecta of several tens of meters would be eroded relatively quickly in geological terms under a warm climate. Therefore, ejecta are an excellent indicator of the degree of preservation of a crater, and will be used as a main parameter in the geomorphic analysis.

[12] A major difference between our geomorphic analysis and previous ones is that new data sets (HRSC, CTX and HiRISE midresolution to high-resolution images) allow us to identify ejecta, which was not possible with Viking data. Indeed, at Viking scale, ejecta are poorly identifiable except when a clear ejecta front is present as for typical lobate ejecta craters [e.g., *Baratoux et al.*, 2005]. With high-resolution imagery it is possible to identify ejecta, even when they are lacking well-defined front, by using indicators such as radial grooves and rays, breccia and local lobes. Reliable identification of ejecta is a major improvement over previous studies for which this parameter was difficult to constrain. In addition to visible imagery, daytime and nighttime near-infrared THEMIS data offer the possibility to identify ejecta from their distinct thermal inertia. This is a result of their difference in physical properties compared to the surrounding terrain, such as grain size and cementation, and the contrast is particularly visible at ejecta terminal lobes [*Baratoux et al.*, 2005]. Hence, we can identify ejecta using multiple parameters and data sets.

3.2. Identification of Fluvial Activity

[13] Fluvial erosion is visible on crater walls and especially on crater rims, because steeper slopes increase the erosional capacity of flowing water, causing incision. On crater walls, slopes are often steep (>10°) and incision is usually limited to subparallel ancient gullies with poor connectivity. These gullies are unrelated to recent gullies, which are fresher and smaller [e.g., *Malin and Edgett*, 2000]. Depositional fans exist at the base of the slope in several cases, as observed by *Moore and Howard* [2005], but their absence does not contradict the presence of fluvial erosion. Indeed, fluvial deposits can have a variety of shapes, with factors such as the presence/absence of a lake in the crater, on the particle size, the bed load, playing a role. In our analysis, we distinguished alluvial fans like those reported by *Moore and Howard* [2005] as a specific parameter in addition to gullied walls, rims and surroundings.

3.3. Classification

[14] *Craddock et al.* [1997] defined five classes of crater degradation progressing from fresh craters to "ghost" craters; craters almost completely removed from the surface. We distinguished only three classes, using two main parameters: the presence of preserved ejecta and of fluvial activity (Figure 3). Thus, the three proposed classes are type I, craters with fluvial erosion on walls and rim but lacking an ejecta blanket; type II, craters with fluvial erosion on walls and rim and a preserved ejecta blanket; and type III, fresh craters lacking any fluvial erosion on rim with a preserved ejecta blanket.

[15] Figure 3 shows an example of each crater type in the NHP region. The type I crater is an 85 km diameter crater with obvious fluvial erosion on the rim (Figure 3a). In this case, fluvial erosion extends far outside the crater (Figure 3c). Fluvial erosion is not obvious on all type I craters and sometimes remains limited to small gullies on rims or valleys in the crater surroundings (close enough to the crater to be superimposed on the former ejecta blanket). Craters with poor rim preservation such as ghost craters (GH in Tables 3 and 4) were interpreted as having been modified by fluvial erosion despite the fact that evidence from images is sometimes poor. These ghost and strongly degraded craters have a shallow depth that may be explained by a volcanic infill. Nevertheless, the observation at high resolution of smoothened rims and valleys at a local-scale favors degradation that occurred before the volcanic infill. Presence of branching valleys in the immediate surroundings of the crater (typically two radii) is also included as a positive indication for fluvial activity after the crater formation. Nowhere around the crater was evidence of an ejecta blanket found in the example in Figure 3a, as well as on all craters classified as type I. Erosion and/or infilling subsequent to the impact have removed all indications of these ejecta from the surface. Most type I craters have flat floors and no central peaks, but these parameters were not used as a tool for classification.

[16] Type II craters are gently degraded craters defined by the combined presence of preserved ejecta and fluvial activity. This does not have to form a continuous ejecta blanket, but a sufficient extent must be preserved to allow formal identification. South of the 62 km diameter crater in Figure 3d, the presence of radial ejecta lobes (Figure 3f) demonstrates that the degree of degradation is clearly less advanced than for type I craters. For type II craters, the rim is locally eroded by fluvial valleys (Figure 3d). Fluvial valleys frequently form alluvial fans at crater floor. Fans can be

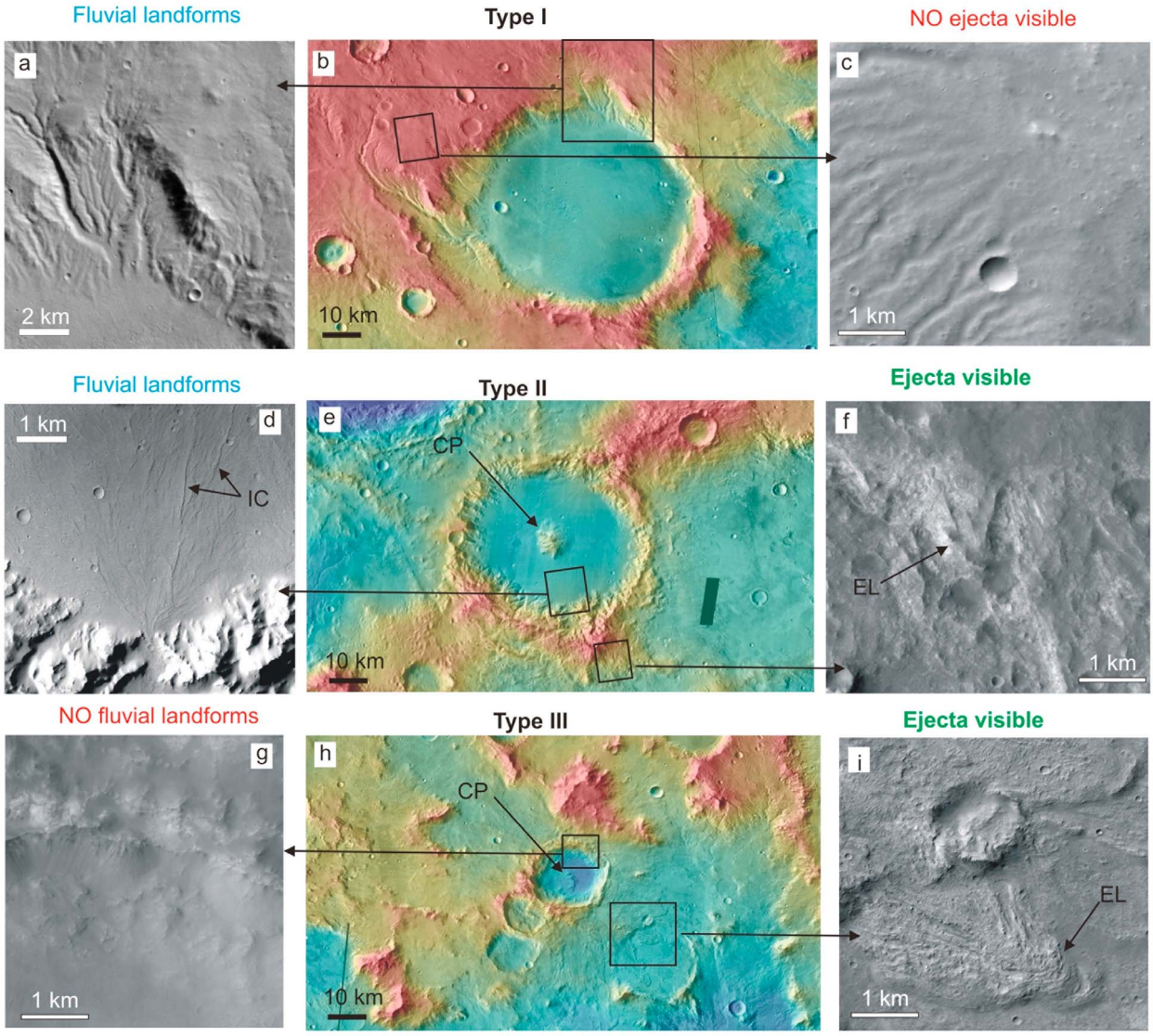


Figure 3. Classification of Martian impact craters from landform identification in the North Hellas Planitia region. Type I (Figure 3b) identified using observations of eroded rims by fluvial landforms (Figure 3a) and lack of visible ejecta all around the crater. Type II (Figure 3e) identified using presence of fluvial landforms, which often include alluvial fans (Figure 3d) and preserved ejecta in locations around the crater (Figure 3f). Type III (Figure 3h) identified by the lack of any fluvial erosion (g) and the presence of preserved ejecta (Figure 3i). (b, e and h) THEMIS mosaic with MOLA data superimposed of craters at respective coordinates of 19°S, 59°E; 23°S, 74°E and 21°S, 70°E. (a) HRSC image. (c) CTX image T01_000884_1611. (d) CTX image P03_002084_1567. (f) CTX image P07_003640_1565. (g) CTX image P06_003416_1600. (i) CTX image P17_007609_1601.

identified by their cone-like shape, their direct association with valleys and/or the presence of inverted channels (IC in Figure 3d) that are characteristic of this landform [*Moore and Howard*, 2005]. The presence of alluvial fans in type II craters is almost systematic compared to type I craters where it is only sparse. As a consequence, we associate type II craters to alluvial fans as classified by *Moore and Howard* [2005]. Last, the common presence of a central peak also indicates the lack of significant infill inside the crater.

[17] Type III craters are the best preserved with usually a complete continuous ejecta blanket (Figures 3h and 3i). Such craters are defined as type III when no evidence fluvial activity was observed on the rim and ejecta. For example, the 32 km diameter crater in Figure 3g has regular slopes typical of granular erosion and dry mass wasting, and well-defined ejecta weakly affected by any erosion process. The type III craters often have central peaks except for some of the smallest.

[18] Unclassified craters are those craters that did not fit into any of the three other groups. In the NHP, we found only one relatively fresh crater (at 29°S) with concentric crater fill and rough deposits suggesting water ice sublimation and a glacial origin [e.g., *Squyres*, 1989; *Mangold*, 2003, 2011a; *Levy et al.*, 2010]. Such craters are often

Table 3. List of Craters in North Hellas Planitia (NHP)[a]

Latitude	East Longitude	Name	Diameter (km)	Ejecta	Fluvial Erosion	Type	Central Peak	Alluvial Fans	Comment
−27.92	74.07	Terby	177	no	yes	1	no	yes	
−21.73	73.83		130	no	yes	1	no	yes	GH
−28.03	57.82		116	no	yes	1	no	no	
−21.17	85.07	Millochau	115	no	yes	1	no	no	
−25.33	71.87		98	no	yes	1	no	no	
−24.55	80.93		94	no	yes	1	no	yes	
−18.83	59.17		89	no	yes	1	no	no	
−27.40	83.28		89	no	yes	1	no	yes	
−28.65	56.58		89	no	yes	1	no	yes	
−24.00	79.37		81	no	yes	1	no	no	
−25.53	53.08		77	no	yes	1	no	no	GH
−21.03	60.78		74	no	yes	1	no	yes	
−17.30	82.78		71	no	yes	1	no	no	
−21.13	67.48		71	no	yes	1	no	yes	
−26.28	84.43		69	no	yes	1	no	no	GH
−22.13	59.80		69	no	yes	1	no	no	
−21.68	53.25		68	no	yes	1	no	no	
−18.68	68.53		63	no	yes	1	no	no	
−26.10	51.90		62	no	yes	1	no	no	
−21.33	76.47		62	no	yes	1	no	no	
−23.02	60.68		60	no	yes	1	no	no	
−24.15	64.98		58	no	yes	1	no	no	
−20.32	59.47		54	no	yes	1	no	no	
−28.47	53.77		53	no	yes	1	no	no	
−24.93	67.07		53	no	yes	1	no	no	
−19.47	66.22		52	no	yes	1	no	no	
−30.00	73.40		52	no	yes	1	no	no	
−29.75	77.78		52	no	yes	1	no	no	
−19.57	84.37		50	no	yes	1	no	no	
−19.43	52.05	Cankuzo	48	no	yes	1	no	no	
−28.87	65.55		47	no	yes	1	no	no	GH
−21.28	86.53	Jumla	44	no	yes	1	no	no	
−26.72	58.20		44	no	yes	1	no	no	GH
−21.45	75.55		43	no	yes	1	no	no	GH
−18.60	82.08		42	no	yes	1	no	no	
−17.52	80.50		42	no	yes	1	no	no	
−21.65	57.63		42	no	yes	1	no	no	
−29.87	83.68		41	no	yes	1	no	yes	
−29.68	82.95		41	no	yes	1	no	no	GH
−25.42	62.05		41	no	yes	1	no	no	
−21.67	77.60		41	no	yes	1	no	no	
−20.00	84.07		40	no	yes	1	no	no	
−18.07	82.15		39	no	yes	1	no	no	
−24.77	59.17		39	no	yes	1	no	no	
−20.22	80.68		39	no	yes	1	no	no	
−30.00	76.12		39	no	yes	1	no	no	
−19.72	75.72		37	no	yes	1	no	no	
−21.62	83.72		37	no	yes	1	no	no	
−24.08	78.25		37	no	yes	1	no	no	
−28.23	52.17		37	no	yes	1	no	no	GH
−26.15	61.23		37	no	yes	1	no	no	
−22.13	68.07		36	no	yes	1	no	yes	
−22.15	70.67		36	no	yes	1	no	no	GH
−26.23	62.45		35	no	yes	1	no	no	
−27.20	65.97		35	no	yes	1	no	no	
−17.13	76.40		35	no	yes	1	no	no	
−27.15	51.95		34	no	yes	1	no	no	
−22.70	75.95		34	no	yes	1	no	no	GH
−26.50	63.38		34	no	yes	1	no	no	
−23.13	84.80		33	no	yes	1	no	no	
−27.45	69.82		32	no	yes	1	no	no	
−26.87	68.45		32	no	yes	1	no	no	
−19.23	72.62		31	no	yes	1	no	no	
−20.03	76.77		31	no	yes	1	no	no	
−29.85	79.53		31	no	yes	1	no	no	
−26.38	64.90		31	no	yes	1	no	no	
−25.87	83.07		30	no	yes	1	no	no	
−20.28	71.03		30	no	yes	1	no	no	
−27.77	83.82		29	no	yes	1	no	yes	
−22.60	79.37		29	no	yes	1	no	no	
−29.98	56.83		29	no	yes	1	no	no	
−23.33	86.08		29	no	yes	1	no	no	

Table 3. (continued)

Latitude	East Longitude	Name	Diameter (km)	Ejecta	Fluvial Erosion	Type	Central Peak	Alluvial Fans	Comment
−29.45	86.27		29	no	yes	1	no	no	
−18.25	79.75		29	no	yes	1	no	no	
−21.38	79.25		28	no	yes	1	no	no	
−24.33	63.63		28	no	yes	1	no	no	
−19.13	84.22		27	no	yes	1	no	no	
−26.57	62.92		27	no	yes	1	no	no	
−21.82	79.98		27	no	yes	1	no	no	GH
−28.35	58.35		27	no	yes	1	no	no	
−27.60	65.47		27	no	yes	1	no	no	
−25.08	83.28		26	no	yes	1	no	no	GH
−26.48	62.27		26	no	yes	1	no	no	
−29.52	62.10		26	no	yes	1	no	no	GH
−22.58	83.47		26	no	yes	1	no	no	
−23.22	64.50		26	no	yes	1	no	no	
−19.90	67.78		25	no	yes	1	no	yes	
−17.25	75.60		25	no	yes	1	no	no	
−30.50	82.12		25	no	yes	1	no	no	
−24.98	84.93		25	no	yes	1	no	no	
−17.32	80.88		25	no	yes	1	no	no	
−27.42	86.12	Suzhi	25	no	yes	1	no	no	
−25.53	85.17		25	no	yes	1	no	no	
−30.00	78.70		25	no	yes	1	no	no	
−21.62	82.43		25	no	yes	1	no	no	
−18.58	76.13		25	no	yes	1	no	no	
−17.77	52.00		24	no	yes	1	no	no	
−21.03	77.52		24	no	yes	1	no	no	
−22.98	77.27		24	no	yes	1	no	no	
−22.95	78.22		24	no	yes	1	no	no	
−23.70	77.32		24	no	yes	1	no	no	
−29.77	56.40		24	no	yes	1	no	no	
−20.07	80.02		24	no	yes	1	no	no	
−19.32	67.68		24	no	yes	1	no	yes	
−23.97	60.52		24	no	yes	1	no	no	
−24.12	62.12		23	no	yes	1	no	no	
−28.27	86.78		23	no	yes	1	no	no	GH
−24.53	70.08		23	no	yes	1	no	no	
−24.97	86.77		23	no	yes	1	no	no	GH
−17.95	73.37		22	no	yes	1	no	no	GH
−19.23	75.77		22	no	yes	1	no	no	
−17.32	76.77		22	no	yes	1	no	no	
−18.97	54.40		22	no	yes	1	no	no	
−19.83	80.13		22	no	yes	1	no	no	
−26.62	61.77		22	no	yes	1	no	no	
−26.30	53.20		22	no	yes	1	no	no	
−21.63	86.42		22	no	yes	1	no	no	
−24.40	86.58		22	no	yes	1	no	no	
−19.13	66.70		22	no	yes	1	no	no	
−22.07	69.58		22	no	yes	1	no	no	
−20.33	81.18		22	no	yes	1	no	no	
−18.33	66.40		21	no	yes	1	no	no	
−26.15	59.78		21	no	yes	1	no	no	
−22.28	82.02		21	no	yes	1	no	no	
−20.15	57.00		21	no	yes	1	no	no	GH
−23.40	86.42		20	no	yes	1	no	no	GH
−21.75	73.17	Saheki	82	yes	yes	2	yes	yes	
−21.92	66.82	Harris, M P	81	yes	yes	2	yes	yes	
−28.87	84.08		75	yes	yes	2	yes	yes	
−23.03	74.25		64	yes	yes	2	yes	yes	
−18.70	62.63		53	yes	yes	2	yes	yes	
−29.77	81.30		53	yes	yes	2	yes	no	
−29.25	74.53		48	yes	yes	2	yes	no	
−17.35	73.88		46	yes	yes	2	yes	yes	
−22.57	65.42		45	yes	yes	2	yes	yes	
−22.45	76.72		43	yes	yes	2	no	yes	
−26.63	75.97	Runanga	41	yes	yes	2	yes	yes	
−27.17	80.13		36	yes	yes	2	yes	no	
−28.37	83.42		32	yes	yes	2	yes	yes	
−28.25	76.87		28	yes	yes	2	yes	no	
−21.85	55.75		24	yes	yes	2	no	yes	
−30.05	77.48		22	yes	yes	2	yes	yes	
−27.62	61.37		55	yes	no	3	no	no	
−17.58	52.18		33	yes	no	3	yes	no	

Table 3. (continued)

Latitude	East Longitude	Name	Diameter (km)	Ejecta	Fluvial Erosion	Type	Central Peak	Alluvial Fans	Comment
−18.65	84.15		34	yes	no	3	yes	no	
−19.17	64.00		33	yes	no	3	yes	no	
−21.43	70.05		31	yes	no	3	yes	no	
−23.10	81.05		27	yes	no	3	yes	no	
−21.55	80.47		26	yes	no	3	yes	no	
−23.68	85.92		26	yes	no	3	yes	no	
−27.67	51.83		23	yes	no	3	yes	no	
−22.75	83.85		23	yes	no	3	yes	no	
−23.82	52.63		22	yes	no	3	yes	no	
−29.08	58.20		22	yes	no	3	no	no	
−24.43	84.18		22	yes	no	3	yes	no	
−18.12	81.92		22	yes	no	3	no	no	
−23.47	51.27		22	yes	no	3	yes	no	
−19.90	73.32		21	yes	no	3	yes	no	
−24.10	51.72		21	yes	no	3	yes	no	
−21.22	84.38	Okotoks	21	yes	no	3	yes	no	
−25.00	76.83		20	yes	no	3	yes	no	

[a]Names from the official nomenclature when existing. Letters from *Moore and Howard* [2005] and *Kraal et al.* [2008]. GH: ghost crater and strongly eroded craters for which fluvial erosion is assumed as being responsible for the degradation.

observed east of Hellas [e.g., *Crown et al.*, 1992]. This crater was included as type III, because it has no evidence of fluvial activity with visible ejecta. In SMT, we found 14 craters with chaotic terrain in their interior floor, a landform thought to be related to the interaction between ice and surface materials [e.g., *Chapman and Tanaka*, 2002]. This filling impeded careful observation of the interior rim and so we were unable to determine their level of degradation as defined above. They were treated separately in subsequent analysis.

[19] A total of 283 craters were able to be classified according to our scheme. In both regions, a large majority (∼70%) are classed as type I. Type II craters are in equivalent proportion to those of type III. Overall, the frequency of degraded craters dominates fresh craters. This can be explained by the peak in impactor flux during the Late Heavy Bombardment (LHB) in the Noachian period.

[20] Figure 4 is a map showing the distribution of the different crater types. Craters from each type are scattered randomly across each region. There are no concentrations of a particular crater type, which suggests the assumption of a spatially homogeneous degradation at the scale of each studied region is reasonable. In such a classification, fresh craters (type III) should postdate the period of highlands degradation experienced by both types I and II. Type II should also postdate type I craters, because they have preserved ejecta, assuming that degradation was spatially homogeneous across each region studied.

[21] A cross-check of these results with the other parameters in Appendices A and B shows that the presence or absence of a central peak is also consistent with this classification. Many craters of type III (>70%), which by definition have ejecta, also have a central peak. Most type II craters (>80%) have a preserved central peak, too. Most type I craters devoid of ejecta are devoid of a central peak. Thus, the loss of ejecta is strongly correlated to burial of central peaks, suggesting the responsible processes are the same. This correlation is important for understanding the processes which caused the crater degradation. For example, highlands' volcanic flows are usually limited to the locations of lowest elevations such as the crater floor and surrounding low elevated plains but they do not degrade ejecta fully and homogeneously around a crater.

[22] A major result from this analysis is the distribution of alluvial fans according to crater type (Appendices A and B). In terms of morphology, type II craters are much less degraded than all type I craters, because they have both ejecta and central peaks. However, it is mainly the type II craters that have fresh alluvial fans. A comparison of fans in type I and type II craters show that type II craters fan correspond almost exclusively to the *Moore and Howard* [2005] and *Kraal et al.* [2008] identification, with only two exceptions (craters D and W, see Table 3) that appear like degraded craters with fresh fans postdating an initial erosion period. Alluvial fans that are observed in a few type I craters are much more degraded, only partly preserved compared to the fresh fans in type II craters, and belong to another type of much less pristine depositional fans. This is a surprising result, because the presence of alluvial fans suggests an enhanced fluvial activity [*Moore and Howard*, 2005] that we would have expected more for older craters than fresher craters with preserved ejecta.

[23] We now present our quantitative analysis to confirm, or not, the conclusions of this classification and analyze further the different degradation stages; in particular the relationships between type II craters and the two other classes, with regards to the presence of *Moore and Howard* [2005] type of alluvial fans.

4. Quantitative Analysis of Degradation

4.1. Depth-Diameter Relationship

[24] Figure 5 shows the depth-diameter plots for the two study regions. Both areas show similar patterns with a general trend of depth increasing with diameter. In both areas, the three crater types form groups, but the groups do overlap. Type III, which are the youngest craters have the deepest depths for a given diameter, and type I, the shallowest depths. Type II craters lie in between these two other types. Craters containing chaotic terrain in SMT fall across the zones occupied by types I and II. A noticeable difference between the two areas is that type I craters in SMT have a larger spread

Table 4. List of Craters in South Margaritifer Terra (SMT)[a]

Latitude	East Longitude	Name	Diameter (km)	Ejecta	Fluvial Erosion	Type	Central Peak	Alluvial Fan	Comment
−19.74	322.37	Vinogradov	224	no	yes	1	no	no	
−21.85	320.41		108	no	yes	1	no	no	
−16.33	335.12		92	no	yes	1	no	no	
−24.69	337.09	Kasimov	87	no	yes	1	no	no	
−24.40	333.15		87	no	yes	1	no	no	
−20.74	324.24	C	74	no	yes	1	no	yes	
−23.54	346.67		70	no	yes	1	no	no	
−18.40	348.05		70	no	yes	1	no	no	
−27.09	341.72	Kashira	66	no	yes	1	no	no	
−27.23	323.07		63	no	yes	1	no	no	
−26.94	348.93		62	no	yes	1	no	no	
−19.84	331.65		62	no	yes	1	no	no	
−14.05	343.66		61	no	yes	1	no	no	
−19.27	337.24		59	no	yes	1	no	no	
−24.17	344.21		57	no	yes	1	no	no	
−25.74	344.12		60	no	yes	1	no	no	
−23.94	348.72		56	no	yes	1	no	no	
−24.46	342.45	Kantang	54	no	yes	1	no	no	
−24.56	344.93		53	no	yes	1	no	yes	
−23.72	332.59		53	no	yes	1	no	no	
−16.82	332.25		53	no	yes	1	no	no	GH
−18.36	335.85		51	no	yes	1	no	no	
−16.94	322.23		50	no	yes	1	no	no	
−18.80	345.53		50	no	yes	1	no	no	
−17.79	320.22		48	no	yes	1	no	no	
−16.96	337.36		48	no	yes	1	no	no	
−15.62	346.34		47	no	yes	1	no	no	GH
−27.91	332.65	W	46	no	yes	1	no	yes	
−17.76	347.06		45	no	yes	1	no	no	
−27.81	346.18		45	no	yes	1	no	no	
−13.45	334.60		45	no	yes	1	no	no	
−25.42	335.69	Noma	40	no	yes	1	no	no	
−17.38	328.58		39	no	yes	1	no	no	GH
−16.91	323.11		39	No	yes	1	no	no	
−21.49	329.17	Grojec	39	no	yes	1	no	no	
−19.66	346.70		39	no	yes	1	no	no	
−22.36	339.47		37	no	yes	1	no	no	GH
−23.26	342.04	Cartago	37	no	yes	1	no	no	
−18.74	342.37		37	no	yes	1	no	no	
−17.98	324.15		35	no	yes	1	no	no	
−14.68	335.48		34	no	yes	1	no	no	GH
−27.99	341.36		34	no	yes	1	no	no	
−14.79	325.76		32	no	yes	1	no	yes	
−21.63	323.72		32	yes	yes	1	no	no	
−17.23	319.91		32	no	yes	1	no	no	
−21.28	336.00	Nitro	31	yes	yes	1	no	no	
−15.01	340.86		31	no	yes	1	no	no	
−14.94	344.09		31	no	yes	1	no	no	
−16.14	348.38		31	no	yes	1	no	no	
−23.93	329.07		30	no	yes	1	no	no	GH
−23.46	347.77	Milna	29	no	yes	1	no	no	GH
−15.76	323.55		28	no	yes	1	no	no	GH
−25.37	340.33		28	no	yes	1	no	no	
−13.62	344.08		28	no	yes	1	no	no	
−27.96	342.47		28	no	yes	1	no	no	
−18.54	345.09		27	no	yes	1	no	no	
−15.48	343.64		27	no	yes	1	no	no	
−14.01	324.39		27	no	yes	1	no	yes	
−18.56	320.43		27	no	yes	1	no	no	
−24.29	331.49	Revda	27	no	yes	1	no	no	
−24.85	344.16		27	no	yes	1	no	no	
−25.27	342.92	Ruby	26	no	yes	1	no	no	
−14.19	332.65		27	no	yes	1	no	no	
−26.88	349.73		25	no	yes	1	no	no	
−25.91	336.48	Navan	25	no	yes	1	no	no	
−15.58	322.01		24	no	yes	1	no	no	GH
−19.13	323.87		23	no	yes	1	no	no	
−14.45	320.77		23	no	yes	1	no	no	GH
−15.02	327.22		23	no	yes	1	no	yes	
−16.81	342.53		23	no	yes	1	no	no	
−27.02	339.37	Lamas	23	no	yes	1	no	no	

Table 4. (continued)

Latitude	East Longitude	Name	Diameter (km)	Ejecta	Fluvial Erosion	Type	Central Peak	Alluvial Fan	Comment
−27.26	349.64		23	no	yes	1	no	no	
−20.07	324.65		22	no	yes	1	no	no	
−20.10	321.05		22	no	yes	1	no	no	
−13.42	320.55		22	no	yes	1	no	no	
−23.29	340.69	Karshi	22	no	yes	1	no	no	
−13.79	323.67		22	no	yes	1	no	no	
−24.16	331.18	Bogra	22	no	yes	1	no	no	
−20.61	333.42	Glazov	22	no	yes	1	no	no	
−13.51	332.93		21	no	yes	1	no	no	
−24.19	340.89	Seminole	21	no	yes	1	no	no	
−15.39	320.57		21	no	yes	1	no	no	
−26.07	325.86	Holden Crater	157	yes	yes	2	no	yes	
−18.92	340.28	Jones	93	yes	yes	2	yes	yes	
−21.73	320.66	A	80	yes	yes	2	no	yes	
−26.58	331.91	Ostrov	74	yes	yes	2	yes	yes	
−14.65	347.20	UC	46	yes	yes	2	yes	yes	
−18.30	323.03	D	38	yes	yes	2	yes	yes	
−24.66	345.13		38	yes	yes	2	yes	yes	
−14.01	343.41		34	yes	yes	2	yes	yes	
−20.58	342.74	Kansk	34	yes	yes	2	yes	yes	
−23.63	348.37		33	yes	yes	2	no	yes	
−27.55	335.71	Sangar	31	yes	yes	2	yes	yes	
−16.31	339.11		31	yes	yes	2	yes	yes	
−15.15	328.90		24	yes	yes	2	no	yes	
−23.67	337.59	Murgoo	23	yes	yes	2	no	yes	
−18.54	330.67	Lorica	46	yes	no	3	yes	no	
−27.50	347.84		32	yes	no	3	yes	no	
−16.05	341.72		28	yes	no	3	yes	no	
−13.25	338.96		24	yes	no	3	no	no	
−21.89	337.56	Loto	23	yes	no	3	yes	no	
−16.73	331.83		22	yes	no	3	yes	no	
−16.38	323.84		21	yes	no	3	no	no	
−16.34	322.39		21	yes	no	3	no	no	
−25.05	343.50	Dison	21	yes	no	3	no	no	
−17.68	331.08		21	yes	no	3	no	no	
−16.74	343.90		20	yes	no	3	yes	no	
−18.38	334.51		56	yes	no	4	no	no	FF
−16.82	334.27		55	yes	no	4	no	no	FF
−13.43	340.00		51	no	yes	4	no	no	FF
−18.13	320.33		42	no	no	4	no	no	FF
−16.32	328.30		42	no	yes	4	no	no	FF
−18.34	333.73		42	yes	no	4	no	no	FF
−15.53	339.51		41	yes	yes	4	no	no	FF
−16.45	327.31		37	no	yes	4	no	no	FF
−20.64	329.34	Shambe	36	no	no	4	no	no	FF
−13.95	326.70		32	no	no	4	no	no	FF
−20.34	329.23	Sigli	32	no	no	4	no	no	FF
−19.90	333.66	Polotsk	31	yes	no	4	no	no	FF
−19.22	327.65		29	no	yes	4	no	no	FF
−15.25	324.40		26	yes	yes	4	no	yes	FF
−14.25	329.51		24	no	yes	4	no	no	FF

[a]Names are from the official nomenclature when existing. Letters are from *Moore and Howard* [2005] and *Kraal et al.* [2008]. GH: ghost crater and strongly eroded craters for which fluvial erosion is assumed to be responsible for the degradation. FF: craters with fractured floor and polygons.

of depths, in fact there appears to be a distinct group of type I craters that have shallower depths than the rest.

4.2. Crater Wall Slope

[25] In terms of diameter plotted versus slope (Figure 6), the three types show a similar distribution to depth-diameter: for a given diameter, type III have the steepest slopes, type I the shallowest and type II lie between and overlap with, the other two types. Craters containing chaotic terrain in SMT fall across the zones occupied by types I and II. Again there are a number of craters in Margaritifer Terra that have lower slopes for a given diameter than their counterparts in either study area. In general, the crater rim slopes do not exceed 0.5 (i.e., ∼27°) and the slope is in general higher for the smaller craters than for larger ones. This trend is particularly clear if type III and type II are considered together.

4.3. Crater Wall Curvature

[26] When curvature is plotted against diameter (Figure 7), the two areas are different. In northern Hellas, curvature tends to increase with diameter, whereas in Margaritifer there is no obvious trend. In both areas, however, the type III craters have the lowest values (∼0.6), type I the higher values (∼0.7) and type II craters lie in between. Notably

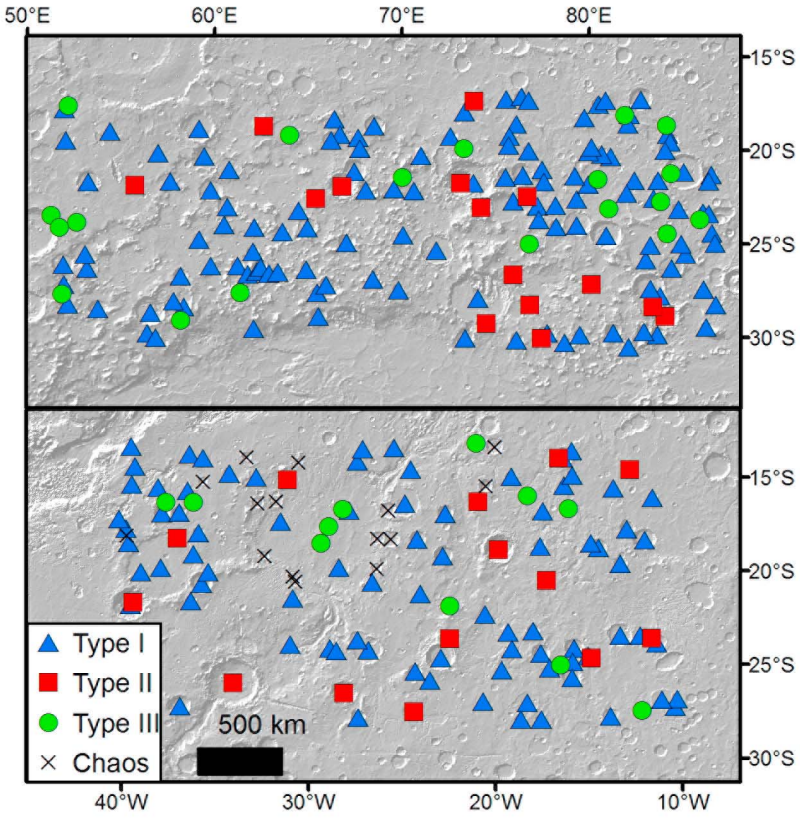


Figure 4. The spatial distribution of the different crater types in each study area. (top) North Hellas Planitia and (bottom) southern Margaritifer Terra. The background is a MOLA hill shade.

southern Margaritifer Terra has several type I craters that have much lower values of curvature than the types I and II for a given diameter, which suggest some of these larger craters have anomalously bowl-shaped interiors.

4.4. Interpretation and Comparison With Previous Studies

[27] *Boyce and Garbeil* [2007] derived a depth-diameter relationship for "pristine" craters; the freshest craters on Mars (Figure 5). *Boyce and Garbeil* [2007] found that the greater the number of shallower, but still fresh craters they included in their estimates the closer their curve moved to that of *Garvin* [2005], who measured fresh craters globally. Both sets of authors used MOLA data on complex craters and measured the depth from the top of the rim to the base of the crater. All of our type III craters plot almost exclusively below the line of *Boyce and Garbeil* [2007], but are scattered about the line of *Garvin* [2005]. This is consistent with their classification as fresh craters and shows they are not unusual compared to the global population of fresh craters. Type II craters tend to plot below the *Garvin* [2005] curve, but above the general trendline our data, also consistent with their classification as slightly degraded. Type I craters are generally found well below the line of *Garvin* [2005], consistent with their degraded nature.

[28] *Craddock et al.* [1997] also studied degraded craters in our study regions, and Figure 5 shows the relationship that they found using photoclinometry on Viking images. Our type I craters are bisected by this curve, showing our results are broadly consistent with those of *Craddock et al.* [1997]. Interestingly our type II craters are almost all positioned above the curve of *Craddock et al.* [1997], showing that they are in general less degraded than those studied by *Craddock et al.* [1997].

[29] Depth-, slope- and curvature-diameter plots (Figures 5–7) all show that the three crater types lie along a morphometric continuum. Crater types I and III form the end-members of this continuum with type II craters lying in between. We know that type III craters are relatively young and unmodified and that type I craters are older and more heavily degraded from our morphological observations. Hence, the morphometric and morphological parts of this study agree and are consistent with the expected aging process for craters. With increasing age and for a given diameter, craters are expected (1) to get shallower, through erosion and infilling, (2) to have higher slopes that degrade to gentler slopes and (3) to become more flat bottomed (from an initial bowl-shaped form) through a combination of 1 and 2. The fact that Figures 5–7 show that type II craters lie between types I and III shows that this crater type is intermediate in the degradation series and therefore implies that this crater type is intermediate in age assuming that these impacts were occurring while modification processes were active. The relatively weakly degraded nature of the

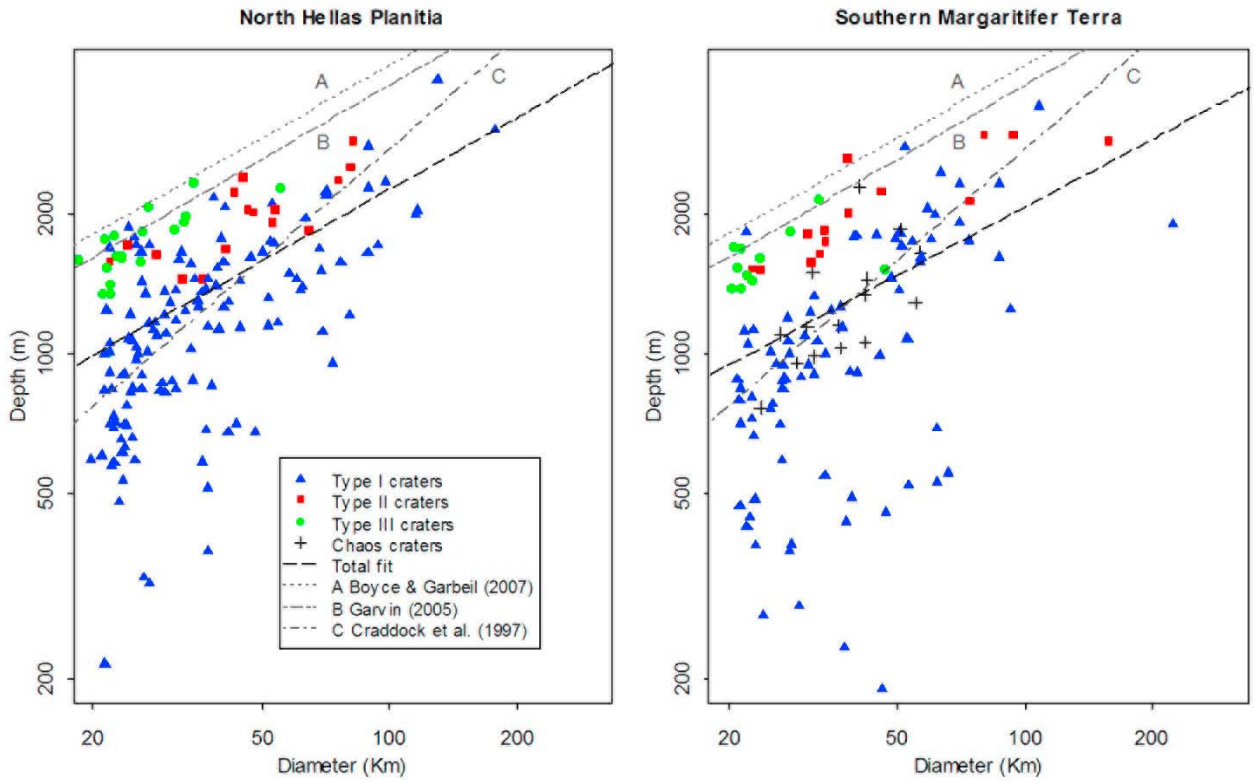


Figure 5. A plot of depth against diameter plot for both study areas with each crater type having a different symbol. Lines A, B and C are depth-diameter relationships derived for pristine impact craters from global MOLA data by *Boyce and Garbeil* [2007], all impact craters from global MOLA data by *Garvin* [2005] and degraded impact craters (combined types B and C) of *Craddock et al.* [1997] in Sinus Sabaeus and Margaritifer Sinus by Viking photoclinometry, respectively.

type II craters is revealed both through the closer proximity of the type II craters to the type III craters on the plots (Figures 5–7) and the proximity of these craters to the fresh global crater curve of *Garvin* [2005].

5. Chronology and Stratigraphy

[30] To obtain an overall chronology of the evolving stages of fluvial erosion on Mars we used both large-scale cumulative crater counts and detailed individual crater counts combined with superposition relationships. From our qualitative and quantitative results we know that type I craters are older than type II, and that type II craters are older than type III. Hence, it is possible to use all of our studied craters and derive ages for each type, by grouping them cumulatively with increasing age and plotting each distribution separately. This analysis assumes that the basement surface is homogeneous in age. The NHP region has a roughly homogeneous basement age, corresponding to post-Hellas, yet early Noachian in age. A regional crater count for each crater type was performed for the NHP region only using the craters listed in Table 3 (section 5.1).

[31] The SMT region has a range of ages for its basement materials (Hesperian volcanic plains overlie the Noachian basement in many places) and a number of chaos floor craters that cannot be classified. Thus, large-scale crater counting could not be used in the same way here. Instead we used small-scale crater counts and superposition relationships on selected craters. Type II craters are the most important to constrain in terms of the chronology. We propose to use this method for selected type II craters in the SMT region (section 5.2). Performing such detailed crater counts for every type II craters would be time consuming and is outside the scope of the present study.

5.1. Chronology of Crater Types in NHP Region

[32] The chronology of all the craters in this region can be performed using classical isochrons as proposed by *Hartmann and Neukum* [2001] and *Michael and Neukum* [2010]. We use the chronology derived from the latter work to estimate the range of ages for each crater type using a cumulative count (Figure 8). The first isochron is derived from all the craters in the NHP region, i.e., using all types. For the second isochron, we removed the type I craters from the analysis, because they are the oldest, to derive an age corresponding to the time at which the first type II craters were emplaced. This should also correspond to the transition into a period with limited crater degradation. Last, the third isochron is derived from a list of type III craters only. This latter curve is less accurate due to the small number of large craters in this group, enabling us to establish an age for craters between 20 and 50 km only. This age corresponds to the time at which major degradation processes ceased and became limited to dry processes.

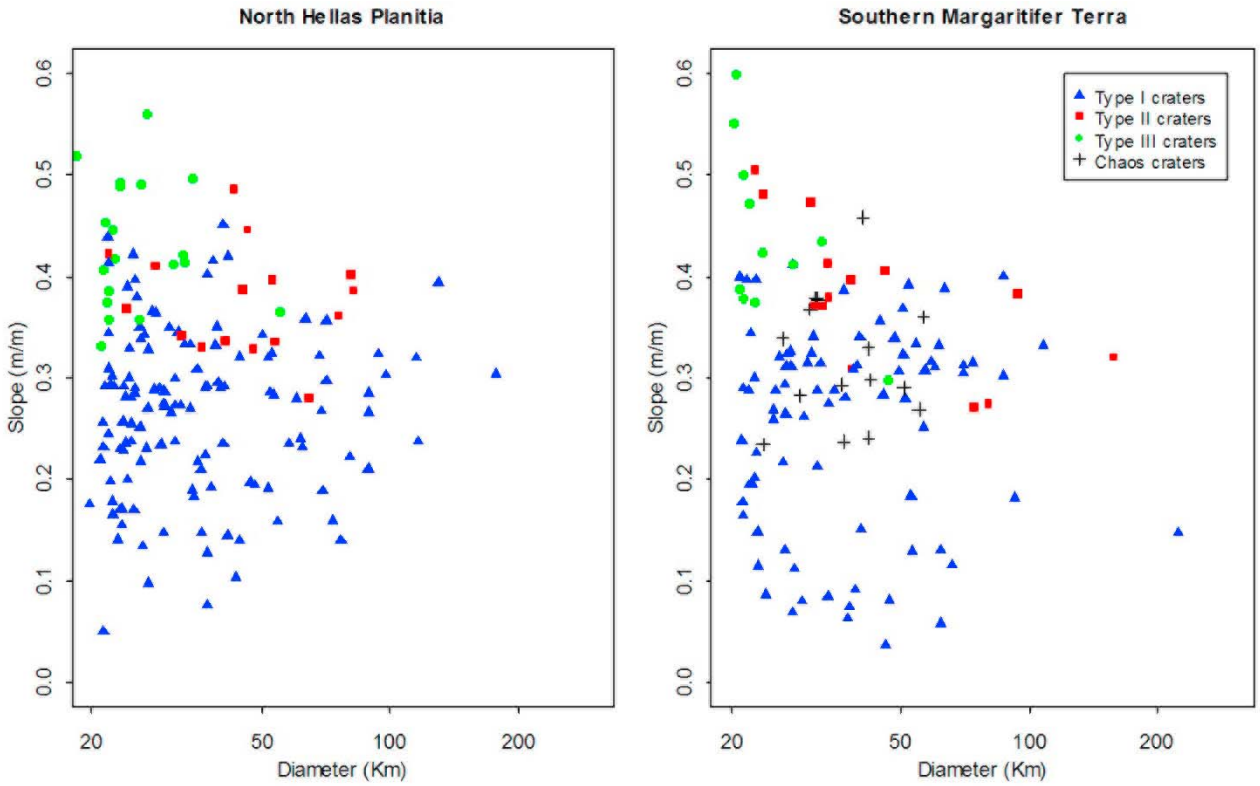


Figure 6. A plot of slope against diameter plot for both study areas with each crater type having a different symbol. For a full explanation of the slope calculation, see section 2.2.

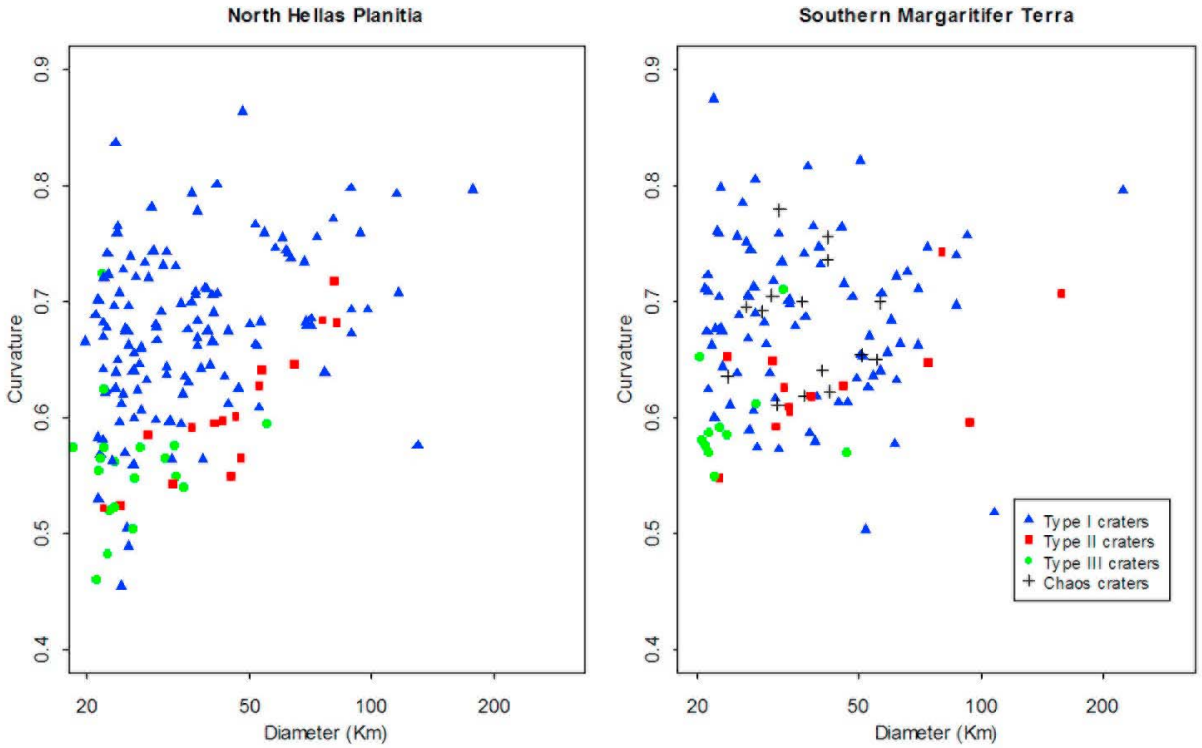


Figure 7. A plot of curvature against diameter for both study areas with each crater type having a different symbol. Values of curvature near 1 are craters that are flat bottomed, values near 0.5 are bowl-shaped, and values near 0 are conical.

[33] Our derived chronology has important implications for the relationship between crater degradation and the evolution Mars' climate. First, all the craters together gives an isochron at 4.00 ± 0.03 Gyr, which corresponds to the age of the basement, therefore to the age of the Hellas basin formation. This age agrees with *Werner*'s [2008] estimation of Hellas' formation at 3.99 ± 0.04 Gyr derived from a similar crater count performed on the western margin of the basin, and that of *Fassett and Head* [2011] at 4.04 Gyr on the northern rim. Note, however, that craters of type I are strongly degraded, thus have a larger apparent crater diameter than the initial crater diameter. This degradation is estimated by *Craddock et al.* [1997] to have increased crater diameters by 10 to 20%. This difference could alter the crater size-frequency distribution and thus changes the derived surface age. This slight modification is estimated using same tools to be between 0.05 and 0.10 Gyr. This does not alter our previous conclusions nor our timeline for this period, but it is of interest that this age becomes closer to the age of the LHB peak measured on lunar samples between 3.85 and 3.9 Gyr [e.g., *Wilhelms*, 1973; *Papike et al.*, 1998]. Indeed, it could reflect that Hellas formation was more coeval to major lunar basin formation than expected.

[34] The transition between type I and type II craters occurs at 3.70 ± 0.06 Gyr, an age corresponding to the middle of the Early Hesperian period in this model age system [*Ivanov*, 2001; *Werner and Tanaka*, 2011]. This age pinpoints the period during which the strong fluvial degradation of Early Mars stopped. This is consistent with recent estimates of valley networks activity cessation in the Early Hesperian [*Fassett and Head*, 2008]. Our derived chronology also shows that the formation of type II craters was sustained over a period ∼0.4 Gyr long during the Hesperian, and stopped at ∼3.32 Gyr. Therefore, type II craters did not form at the end of the Late Noachian, and thus they cannot be the result of the climatic optimum which formed the valley networks at that time [e.g., *Howard et al.*, 2005; *Irwin et al.*, 2005]. If they are related to an enhanced period of erosion, as proposed by *Moore and Howard* [2005], the degradation of these craters would have taken place in a global climatic optimum that occurred close to the end of this period, i.e., Late Hesperian or beginning of Early Amazonian, to explain all type II craters degradation. Alternatively, these craters are not a result of an enhanced period of erosion but of climatic episodes of limited amplitude and/or regional extent scattered along the 0.4 Gyr period or regional processes related to local conditions, such as, episodic climate warming triggered by crater formation.

[35] The transition between type II and type III is dated at ∼3.32 +0.12/−0.34 Gyr, i.e., at the beginning of the Early Amazonian in this age system. This age is not as tightly constrained as the previous ones, and there are several plausible interpretations for this age. For example, if the degradation of type II craters is dependent on their diameter, as could be the case for regional warming triggered by crater formation [e.g., *Segura et al.*, 2002, 2008], then it is possible that the formation of type II craters extends later and that smaller type III craters could have been emplaced before. In other words, we cannot be sure that all type III craters postdate all type II craters, assuming that type II degradation is not a global phenomenon nor related, for example, to the availability of ice in the impacted region. The depletion of large craters of type III may be correlated to such effect.

5.2. Age of Selected Type II Craters in SMT Region

[36] Jones crater is an 85 km diameter complex crater located in the east of the SMT region (19°S, 341°E). Jones has fresh ejecta visible on a range of types of imagery (Figure 9). THEMIS daytime and nighttime mosaics show chains of secondary craters, rays and lobes all around the crater. Higher resolution images are sparse around Jones, but where available show rough terrain with many small elongated and irregular secondary craters. A geomorphic map of the Jones' ejecta (Figure 9b) has been assembled using all available imagery. Ejecta can be difficult to identify with certainty in places, so the boundary marked on Figure 9b is only approximate and based on the most distal ejecta lobes that we found. This map shows that these ejecta extend about two to three crater radii (2R to 3R) from the crater center, typical for this size of crater [e.g., *Barlow*, 2005].

[37] Jones crater has a 20 km wide alluvial fan in its northern section and local fluvial dissection elsewhere (Figure 10). We classified it, therefore, as a type II crater, i.e., as possessing ejecta and fluvial activity. Jones is very near two important Martian valley networks, Samara Vallis to the south and Loire Vallis to the east. Both valleys dip toward the northwest, following the regional slope. An important observation is that the Jones' ejecta covers both valley systems, demonstrating that Jones postdates the fluvial activity of both valleys, which have been dated as Late Noachian–Early Hesperian [*Carr*, 1996; *Fassett and Head*, 2008]. This crosscutting relationship is particularly visible in the case of Loire Vallis. This valley cuts the Noachian plateau and has many small side tributaries all along its length to the east of the Jones' ejecta. When it reaches the Jones' ejecta, the valley seems to disappear in the visible images, but a shallow, subdued valley remains in the topographic data. No valley appears to cut ejecta at high resolution (Figure 10e). North of the Jones' ejecta the valley reappears, and then is blanketed by another fresh crater's ejecta. The thickness of the ejecta of an 85 km diameter crater should be in the range of 100–200 m between 1R and 2R from the crater center [*McGetchin et al.*, 1973]. Such a thickness is consistent with the smoothing of Loire Vallis, which has a depth of 200–500 m upstream Jones crater. We also found a small valley (SV on the map Figure 9b) that seems to postdate Jones crater and joins the buried Loire Vallis valley (dotted lines) suggesting a small reactivation of this valley after the Jones crater formation.

[38] To the south, Samara Vallis displays similar morphology to Loire Vallis, and also cuts the Noachian plateau. Beneath the Jones' ejecta this valley is only occasionally visible, either in topographic or image data. It cannot be followed continuously through the ejecta. Nevertheless, in the western section of the ejecta, a fresh valley with braided morphology (BV) is clearly visible at the location of the former Samara Vallis. This braided morphology is distinct from the southern section of Samara Vallis, suggesting that, here too, the fresh valley is a reactivation, and does not correspond to the Samara Vallis in a strict sense. The braided morphology advocates a short-term episode. Damming from the ejecta and local outburst from melted snow or ground ice generated by the impact itself could explain this fluvial

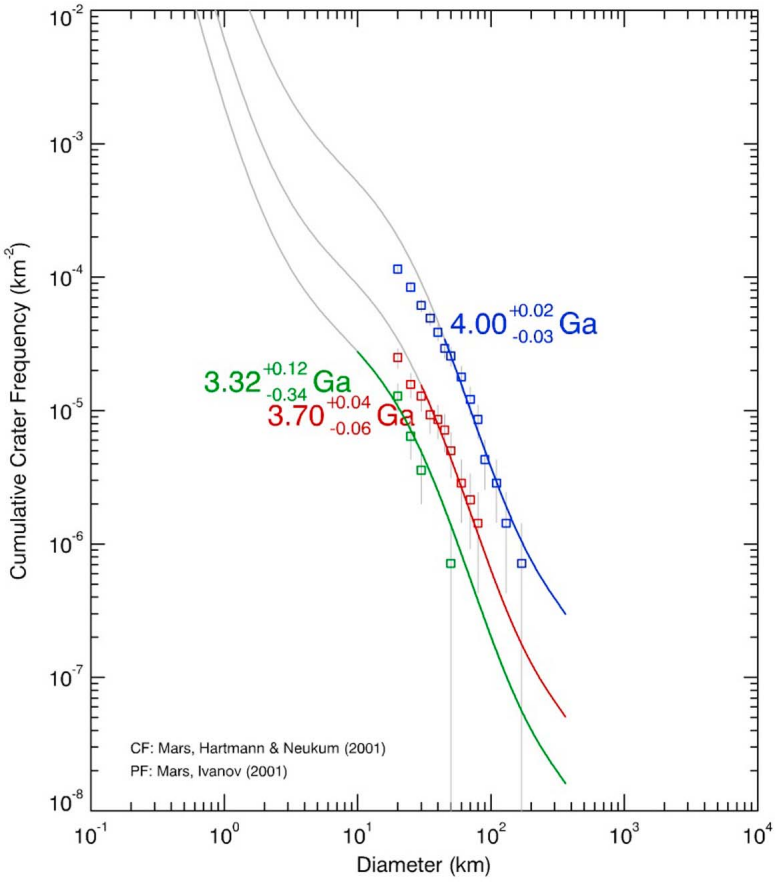


Figure 8. Chronology of crater degradation at north Hellas Planitia using *Michael and Neukum*'s [2010] tools. Age in black is obtained from plotting all craters. Age in red is obtained by removing type I craters. Age in blue is obtained by removing both types I and II. The period defined by blue and red curves accounts for type I crater formation. The period defined by red and green curve accounts for type II crater formation. Fresh craters formed after age in green. Isochron in blue is obtained for craters >40 km (shift of smaller craters below isochron due to small craters degradation). Isochron in red is obtained for >25 km. Isochron in green is obtained with all craters sizes.

landform [*Jones et al.*, 2011; *Mangold*, 2011b]. The lack of dissection of Jones' ejecta shows that this crater postdates the period of intense fluvial activity on Mars.

[39] We performed crater counts on the ejecta blanket to estimate the age of Jones crater. We only counted well-rounded fresh craters, and avoided the few elongated rays of Jones' secondaries that cover part of the ejecta surface. This crater count reveals that Jones crater was formed in the Late Hesperian (Figure 11). Indeed, the density of craters >1 km on the 5300 km^2 surface is N(1) = 2260 ± 650 craters/10^6 km^2 (see Table 5). This density puts the age of the crater in the Late Hesperian epoch according to the *Werner and Tanaka* [2011] stratigraphy. The graph adapted from *Michael and Neukum* [2010] shows the distribution of craters from 700 m to 4 km. There is a shift from model isochrons below 1 km, as usually observed in case of resurfacing [e.g., *Hartmann and Neukum*, 2001]. This would limit any further attempt for obtaining a better statistical plot using smaller craters. In the crater count plot, the regression curve for craters larger than 1 km displays an age at 3.60 +0.06/−0.10 Gyr in *Ivanov*'s [2001] model that also corresponds to the Late Hesperian epoch, at the beginning of this period that extends from 3.65 to 3.46 Gyr in this model (Table 5). In summary, the type II Jones crater formed in the Late Hesperian. It has alluvial fans, sparse fluvial landforms on its rim, and a couple of fresh valleys on its ejecta, that all postdate the crater formation. Most of the regional fluvial activity predates Jones crater, and did not reincise the ejecta after its formation, apart from small local reactivations inside the ejecta.

[40] Another unnamed crater, hereafter named UC, is studied in Figure 12. It displays well-preserved ejecta blanket visible in THEMIS nighttime images as well as in visible imagery. The ejecta cover an ancient fluvial valley at its northwestern edge (V in Figure 12a). Alluvial fans and fluvial valleys are observed on inner rims and floor. This 45 km diameter crater is therefore classed as a type II. Ejecta have been used to count craters, using two 600 km2 areas on each side of the crater along a CTX image. Results show a best fit at 3.43 Ga +0.07/−0.12 Ga suggesting an age in the Late Hesperian epoch. A Late Hesperian age is also consistent

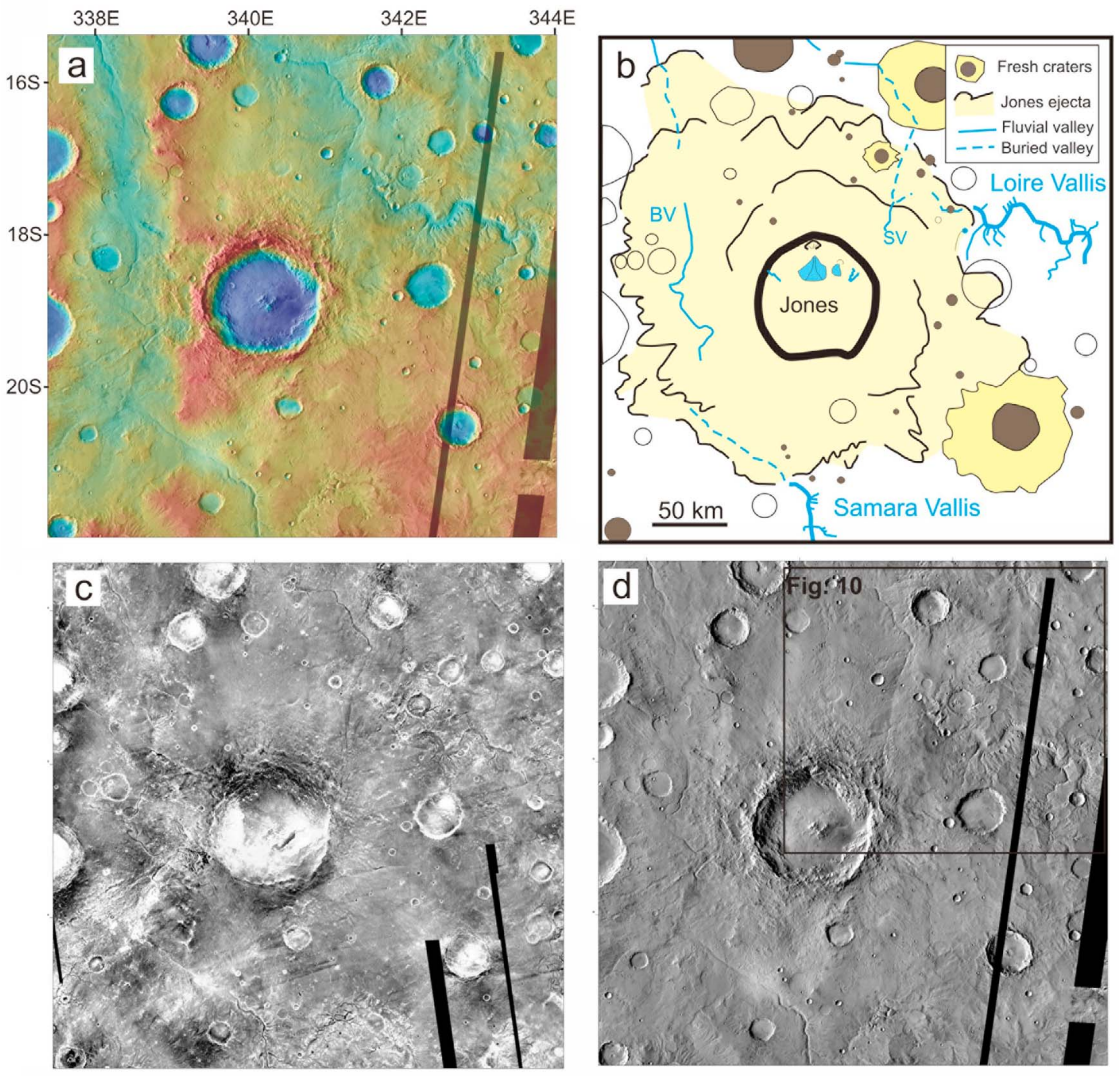


Figure 9. The 85 km diameter Jones crater (19°S, 341°E). (a) THEMIS daytime image with MOLA topography superimposed showing Jones in the center. (b) Geomorphic map of Jones crater and ejecta with fluvial landforms indicated in blue. Dotted lines show how the main valleys are buried by ejecta with only little reactivation at SV and BV. SV, Small valley; BV, Braided valley. (c) THEMIS nighttime mosaic from which ejecta lobes are clearly visible. (d) THEMIS daytime mosaic. The scale in all figures is as indicated in Figure 9b and north is up.

with a N(1) = 2500 ± 1400 craters/10^6 km^2, but the statistics of >1 km craters is limited to three craters.

[41] Of interest is also the well-known Holden crater [e.g., *Grant et al.*, 2008]. This 150 km diameter crater has been mapped as a type II crater because of the presence of well-developed alluvial fans combined with visible ejecta particularly on its northern side. A recent study has shown that Holden's ejecta postdate the formation of most of the regional fluvial landforms including valley networks, but predate the formation of the Eberswalde depositional fan, which is located inside the ejecta blanket, and, similarly, Holden crater is dated to the Hesperian, postdating the early Mars' intense fluvial activity (N. Mangold et al., The origin and timing of fluvial activity at the Eberswalde crater, Mars, submitted to *Icarus*, 2012).

[42] In the SMT region, we found no type II craters that are crosscut by ancient valley networks, suggesting that they are all younger than the Late Noachian/Early Hesperian period. These results on individual craters in SMT confirm the age obtained from the regional count in NHP. Thus, the processes responsible for both the alluvial fans and reactivated valleys observed for type II craters are not the same as those active on early Mars, the period of activity of valley networks, but could be due to local processes produced by the impact itself [e.g., *Jones et al.*, 2011; *Mangold*, 2011b, 2012] or an episodic climatic warming postdating the formation of type II craters in the Late Hesperian [*Mangold et al.*, 2008; *Grant and Wilson*, 2011].

6. Discussion

[43] The classification of craters into three different types has enabled us to derive ages for their respective periods of formation, that delimit three main periods in Mars' history

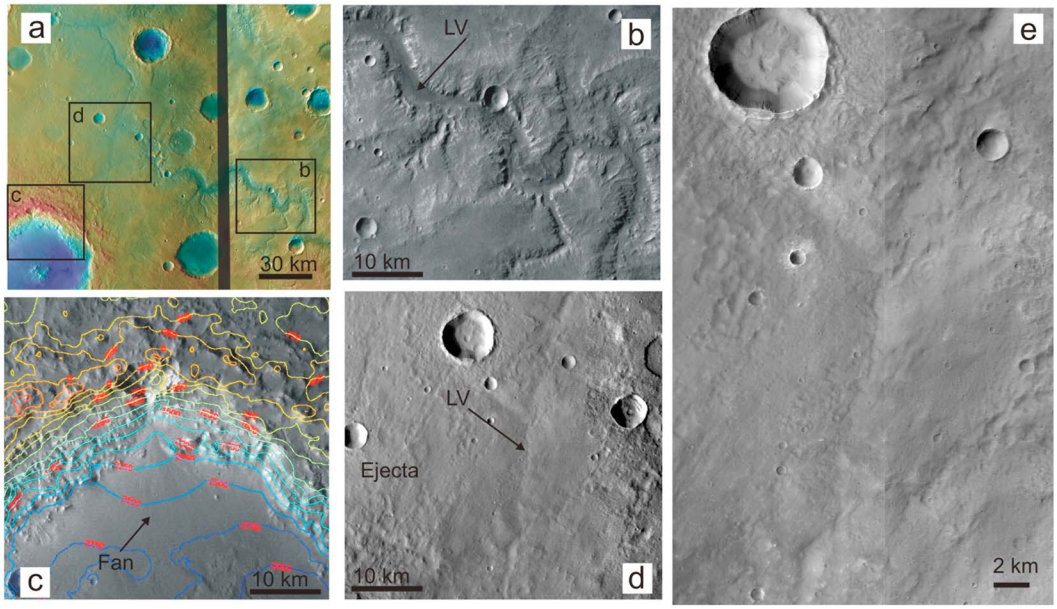


Figure 10. Crosscutting relationships of Jones crater with fluvial landforms. (a) HRSC view of the NE of Jones crater with MOLA topography superimposed (images from orbit 4090, 7190 and 7215). (b) Close-up of HRSC (orbit 4090) image on Loire Vallis (LV) showing strong erosion by fluvial landforms. (c) HRSC image (orbit 7215) with MOLA contours superimposed of the main alluvial fan inside Jones crater. (d) HRSC image (orbit 7190) of the ejecta of Jones with the Loire Vallis (LV) or one of its tributaries smoothed by the ejecta. (e) Close-up inside Figure 10d using CTX images B20_017528_1632 and B11_013849_1631 over the topographic low corresponding to the former Loire Vallis or one of its tributaries. Material corresponds to Jones ejecta grooves, rays and secondaries; no fresh fluvial incision is observed. North is up in all images.

(Figure 13). The following discussion explores the wider context and implications of these results.

6.1. Large Alluvial Fans as Indicator of Hesperian Late Stage Conditions

[44] Our chronology shows that type II craters formed from the Early Hesperian to earliest Amazonian epochs that are known to have been significantly colder than the Noachian period [e.g., *Carr and Head*, 2010]. Nevertheless, evidence of fluvial activity during this period has been reported in a number of locations: on flanks of several volcanoes where it was almost certainly caused by hydrothermal activity triggered by volcanic events [*Gulick and Baker*, 1990]; in Hesperian terrains such as in Valles Marineris chasmata and plateau [*Mangold et al.*, 2004, 2008, *Quantin et al.*, 2005], or in ancient terrains such as in Naktong and Parana Vallis [*Bouley et al.*, 2009, 2010], Claritas Fossae [*Mangold and Ansan*, 2006] or in Newton crater [*Howard and Moore*, 2011] where it was likely related to regional fluvial activity. Recently, *Grant and Wilson* [2011] showed that alluvial fans, like those in our type II craters, have Late Hesperian to Early Amazonian ages based on small impact crater counts on these fans. While they suspect the activity to have occurred much later than the formation of the host craters, some or all of these craters could have formed late enough to fit with our chronology (Figures 8 and 13). Our results confirm their conclusion that the fans formed during a late stage of fluvial activity. Thus, late stage fluvial activity occurred in this period of early Mars, but with an amplitude

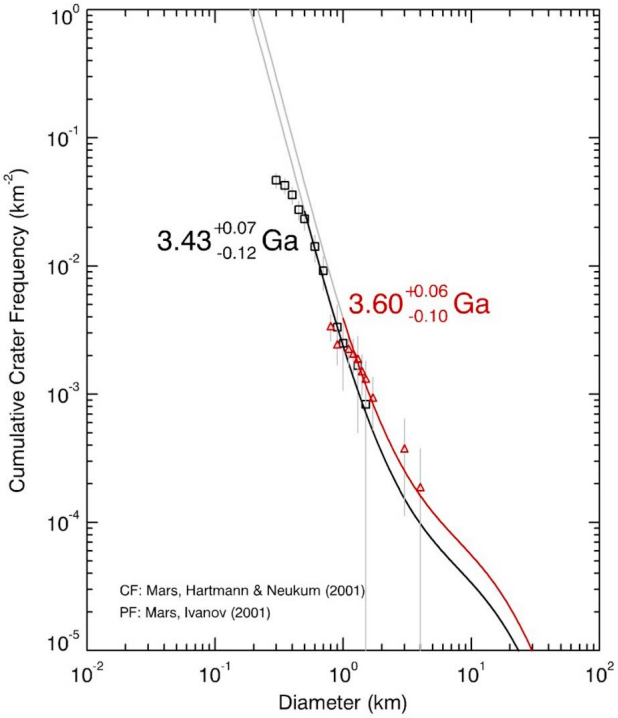


Figure 11. Crater count with isochron estimation of Jones crater ejecta blanket in red using craters >1 km [after *Michael and Neukum*, 2010]. In black, isochron of unnamed crater UC using craters >500 m.

Table 5. Crater Frequencies and Their Model Absolute Ages for Lower Boundaries of Martian Epochs at Specific Crater Diameters in Cumulative Numbers[a]

	Model Ages (Ga)		N(1)		
Epoch Boundaries	b	c	a	b	c
Middle to Late Amazonian	**0.39**	0.23	160	160	160
Early Mid-Amazonian	**1.45**	0.88	600	600	600
Hesperian–Amazonian	**3.46**	3.00	2100	2100	2100
Early Late Hesperian	**3.65**	3.40	3125	4050	3067
Noachian–Hesperian	**3.74**	3.57	5000	6481	4097
Middle to Late Noachian	**3.86**	3.85	25600	12667	19315
Early Mid-Noachian	**3.97**	3.96	51200	25334	38630

[a]For the fits, different size-frequency distribution shapes were used: shape a, a −2-slope power law as in the work by *Werner and Tanaka* [2011]; shape b, the description of *Ivanov* [2001]; and shape c, a cumulative version of the description by *Hartmann* [2005]. The age is derived from the chronology model of *Ivanov* [2001] (shape b) and derived from *Hartmann* [2005] (shape c). See *Werner and Tanaka* [2011] for details. Model ages used in our study are in bold.

much smaller than in the Noachian period, which implies colder conditions with only transient melting.

[45] It is important to note that type II alluvial fans are quite similar to one another, in terms of morphology and size. If these fans were formed under continuous climatic conditions, the older craters should be much larger and thicker than the younger ones, contrary to observations. Only Holden crater seems to show the most developed fans, but this is also the largest crater in the list of type II craters. Alternatively, the relative similarity in fan shape could be due to regional variations or several episodes over time, or to the impact itself, which would have generated by a single regional episode. *Armitage et al.* [2011] studied alluvial fans geometry in order to determine their lifetime. They concluded, for the largest ones in Holden crater, that two scenarios were possible, either (1) rates of precipitation that are similar to arid terrestrial climates over timescales of 10^7 to 10^8 years or (2) a shorter duration of semiarid to temperate climate conditions over a period on the order of 10^6 years. From our results, we would favor the second interpretation with a regional or a short-scale globally warmer and wetter climate inside a generally cold period in the Hesperian.

[46] Recent modeling of outflow channel water release and lake formation shows that regional snow deposition and subsequent melting is possible over limited time periods, which can explain localized fluvial activity on the Valles Marineris plateau [*Kite et al.*, 2011]. This process is only valid close to lacustrine activity, or to the outflow channel release. This process could have occurred in the SMT region where outflow channels such as Uzboï released water during the Hesperian [e.g., *Grant et al.*, 2008], but not in the NHP region where no such activity has been observed. Nevertheless, such process was proposed to have occurred at a global scale as a result of the main period of outflow channel formation in the Late Hesperian [*Baker et al.*, 1991], a timing that is consistent with the type II crater ages.

[47] Alternatively, as mentioned by *Moore and Howard* [2005], impact events can create significant warming, which can cause the melting of subsurface ice or surface snow [*Segura et al.*, 2002, 2007, 2008; *Toon et al.*, 2010]. Recent identification of alteration minerals at the base of alluvial fans in some northern Hellas craters suggests snowmelt by impact warming is a possibility [*Mangold et al.*, 2011; N. Mangold et al., Aqueous alteration of a Late Hesperian Majuro crater, Mars, submitted to *Planetary Space Science*, 2012].

[48] Conditions that formed alluvial fans are therefore not necessarily related to a climate that is warmer than today, but to local or regional conditions which require only two factors: (1) water ice should be present in the subsurface, or should fall as snow, in order to explain the fluvial activity by local melting; and (2) snowmelt should not evaporate too fast, suggesting these fans formed during periods of higher atmospheric pressure than current ones. Thus, alluvial fans in type II craters may represent, not a climatic optimum in early Mars, but transient processes in the late stages of early Mars with cold conditions but still a higher atmospheric pressure than in current conditions.

6.2. Implications of the Quick Transition From Type I to Type II Craters

[49] Type II craters are distinguishable from type I craters by the presence of ejecta, but also by the presence of alluvial fans, which are not found in type I craters. Here, we explain how the transition between these two craters types may highlight a global shift in climatic conditions.

[50] First, we can assume that the erosion of the type II craters was due to regional activity. The distinct

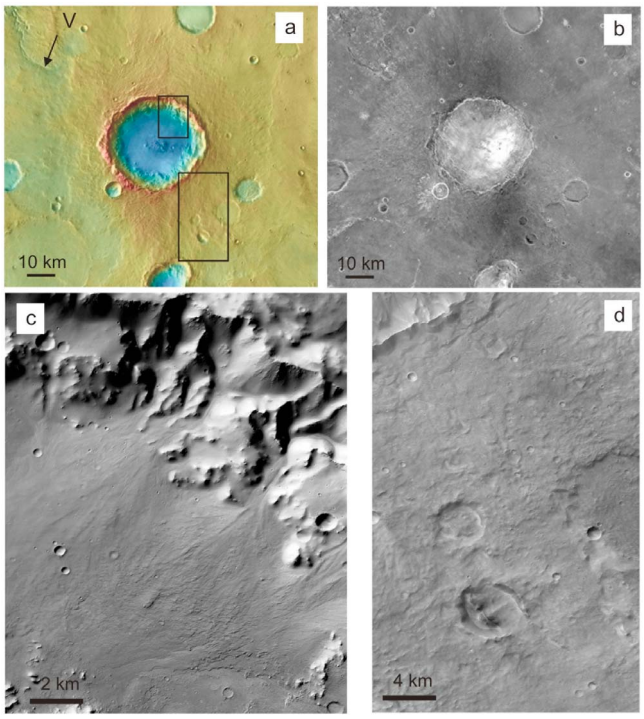


Figure 12. Unnamed 45 km diameter crater UC located 14°S, 347E. (a) Daytime THEMIS mosaic superimposed with MOLA elevation in color (from −2500 m in blue to −500 m in red). (b) Nighttime THEMIS mosaic. (c) Inner rim with alluvial fans shown by CTX P_22_009827_1653. (d) Close-up on ejecta blanket with CTX P12_005898_1660. Notice that the two ∼5 km diameter craters in the center have been blanketed by the ejecta.

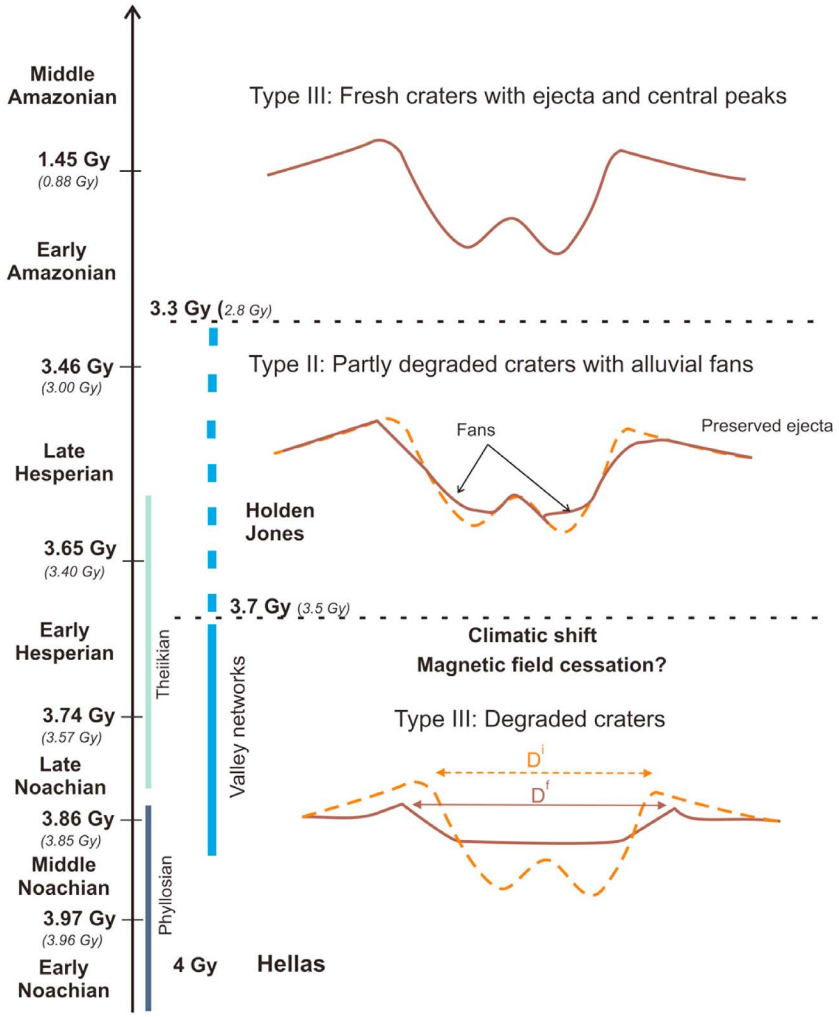


Figure 13. Martian timescale with the three types of craters defining three different epochs. Dotted lines in type I and II indicate fresh craters morphology as for type III. D^i and D^f indicate initial diameter and final diameter after degradation, respectively. Ages in normal font correspond to *Ivanov* [2001] production function, and ages in italic correspond to Hartmann function (see *Hartmann and Neukum* [2001] for details).

morphologies of type I and type II could be the result of global processes which were active during type I crater formation and degradation, followed by a sudden shift in climate conditions and subsequent regional activity related to the presence of ice and to the craters themselves. This would have led to a strong transition dated by the end of type I craters at ~3.7 Gyr.

[51] Second, we can assume global erosion processes for all degradation. If the same style of fluvial activity eroded both the type I and type II crater rims, one would expect that the same landforms would have developed. It is possible that the type I craters were already degraded to such a degree that the potential for subsequent erosion was minimal. So, the lower intensity degradation of type II craters may not have modified significantly the type I craters. Alternatively, the fact that we see different morphologies in the two crater types could suggest two different styles of fluvial activity occurred, which could be a result of substantially different climatic conditions, i.e., if alluvial fans formed under cold conditions and mainly by snowmelt whereas type I were degraded under a warmer climate. In both cases, the type II erosion is more limited, postdates most valley network formation, and thus represents a more moderate level of erosion compared to type I craters.

[52] In addition, there are apparently only a few craters at the transition between the two types. Assuming the type I and II craters form a continuum of degradation resulting from a changing climate, this observation is important because it shows that the transition responsible for the change in degradation between types I and II is sharp. This interpretation is discussed below considering the observations from the crater depth to diameter plot (Figure 5). Type II craters are deeper than type I craters on average (Table 2), but several type I craters have a depth similar to that of type II craters, i.e., about 15 craters in NHP and 10 craters in SMT. This corresponds to roughly 15% of the type I craters. Statistically, some of these craters could have been slightly deeper initially and may have preserved some of this initial

depth even after degradation, but this could not account for all of these craters. Therefore, there is a number of type I craters that display geometric degradation no stronger than that shown by type II craters. However, they are different to type II craters, because of the lack of visible ejecta, thus suggesting a higher erosion rate occurred after their formation. As a consequence, these relatively weakly degraded type I craters could represent the last gasp of the intense fluvial activity during early Mars period, thus during the last tens of millions years of this period.

[53] Assuming that our interpretation of a sharp climate shift is valid, what could be the cause of this shift? A similar shift was proposed to explain the transition from alteration minerals dominated by phyllosilicates in the Noachian crust toward more sulfate-dominated alteration in post-Noachian sediments [*Bibring et al.*, 2006]. This transition has been attributed to a progressive drying out and acidification of the surface of the planet. Our results are consistent with this paradigm, with the difference that our shift may be a sharp rather than a progressive climate change, and the timing of the shift occurs after the start of sulfate formation (Figure 13), which is reported to have started in Meridiani in the Late Noachian [e.g., *Hynek et al.*, 2002] and supposed to have stalled progressively by the middle of the Hesperian [*Bibring et al.*, 2006]. A similar implication was made by *Fassett and Head* [2008], who found that the formation of valley networks ended sharply in the Early Hesperian.

[54] A sudden modification in climate could be due to a sudden change in the rate of atmospheric escape. This could be explained by a transition from a period during which the atmosphere is protected by the magnetic field, to one where the magnetic field is absent, allowing more efficient atmospheric loss through non thermal escape [*Chassefière et al.*, 2007]. The very different magnetic signatures of basins larger than 1000 km and similar in age led to the conclusion that the Martian dynamo stopped at ∼4.1 Ga [*Lillis et al.*, 2008]. This early timing is however inconsistent with the magnetization associated with late Noachian volcanoes such as Apollinaris, Hadriaca and Tyrrhena Paterae [*Lillis et al.*, 2006; *Langlais and Purucker*, 2007; *Hood et al.*, 2010]. A study based on the statistical analysis of several independent models using MGS measurements found that the magnetic field features associated with Noachian and Hesperian units were very similar [*Milbury and Schubert*, 2010], suggesting that the dynamo could have been active during these two epochs. A recent study focused on 250–800 km impact craters and on Hesperian volcanoes showed that the dynamo may have stopped between 3.75 and 3.79 Gyr, well after the Hellas impact [*Langlais et al.*, 2011, 2012]. This event may have caused a sudden climatic shift, which may have provoked the sharp shift in crater degradation conditions that we have detected at the end of the Early Hesperian.

7. Conclusions

[55] We have analyzed and measured geometric properties of 283 craters of >20 km in diameter in two highland regions of Mars. We have been able to define three main classes of crater, with progressively increasing levels of degradation, both in terms of qualitative morphology and quantitative geometric measurements: Namely from fresh craters with ejecta and central peak (type III), to gently degraded craters with ejecta and often a central peak, with fluvial landforms including alluvial fans (type II), and strongly degraded craters without ejecta or central peak and with fluvial erosion (type I). The main results are as follows:

[56] 1.The geometry of strongly degraded craters confirms qualitative and quantitative studies done at Viking scale that these craters have been highly fluvially modified compared to fresh craters.

[57] 2. Craters with alluvial fans as identified initially by *Moore and Howard* [2005] display preserved ejecta blankets and a depth-diameter ratio closer to fresh craters (type III) than to strongly degraded craters (type I).

[58] 3. The difference in degradation between the three classes of impact craters allowed us to construct a time series showing that craters with alluvial fans (type II) were formed between the Early Hesperian (∼3.7 Gyr using *Ivanov*'s [2001] production function, slightly younger absolute ages would be obtained with Hartmann function), and the Early Amazonian (∼3.3 Gyr), much later than the period during which type I craters were formed and degraded (between ∼4 Gyr and ∼3.7 Gyr). This chronology is corroborated by the crosscutting relationships of type II craters such as Jones and Holden, which are Hesperian and postdate valley networks known to have peaked during the Late Noachian.

[59] 4. As a consequence of the two previous points, type II craters with alluvial fans correspond either to the waning stages of fluvial activity in a globally colder climate than in the Noachian with regional or global episodic warmer periods allowing us to better constrain the Hesperian climate, or, alternatively, regional processes triggered by impact crater formation.

[60] 5. A quick shift in crater degradation is observed between type I and type II craters at the end of the Noachian/beginning of Early Hesperian with only few craters being at the transition at ∼3.7 Gyr. It could be explained by the cessation of the dynamo at a similar epoch or slightly before, at ∼3.77 Gyr [*Langlais et al.*, 2012].

[61] Further work is required to better understand why there is a difference in degradation style between type I craters and type II craters. This transition could help us to understand the difference in climatic conditions between the Noachian and subsequent periods.

[62] **Acknowledgments.** V.A., B.L., and N.M. were supported through ANR-08-JCJC-0126 "MADMACS" and the Programme National de Planétologie (PNP) of Institut National des Sciences de l'Univers (INSU-CNRS) and the Centre National d'Etudes Spatiales (CNES). We acknowledge the effort of HRSC team members who have contributed to HRSC investigations in the preparatory phases, and the use of CTX and HiRISE data available online. N.M., S.C., V.A., and B.L. wrote the paper; S.A. and N.M. produced the classification; S.A. and S.C produced statistics; and N.M and V.A. produced regional mapping and chronology.

References

Ansan, V., and N. Mangold (2006), New observations of Warrego Valles, Mars: Evidence for precipitation and surface runoff, *Planet. Space Sci.*, *54*, 219–242, doi:10.1016/j.pss.2005.12.009.

Ansan, V., N. Mangold, P. Masson, E. Gailhardis, and G. Neukum (2008), Topography of valley networks on Mars from Mars Express High Resolution Stereo Camera digital elevation models, *J. Geophys. Res.*, *113*, E07006, doi:10.1029/2007JE002986.

Ansan, V., et al. (2011), Stratigraphy, mineralogy, and origin of layered deposits inside Terby crater, Mars, *Icarus*, *211*(1), 273–304, doi:10.1016/j.icarus.2010.09.011.

Armitage, J. J., N. H. Warner, K. Goddard, and S. Gupta (2011), Timescales of alluvial fan development by precipitation on Mars, *Geophys. Res. Lett.*, *38*, L17203, doi:10.1029/2011GL048907.

Baker, V. R., R. G. Strom, V. C. Gulick, J. S. Kargel, G. Komatsu, and V. S. Kale (1991), Ancient oceans, ice sheets and the hydrological cycle on Mars, *Nature*, *352*(6336), 589–594, doi:10.1038/352589a0.

Baratoux, D., N. Mangold, P. Pinet, and F. Costard (2005), Thermal properties of lobate ejecta in Syrtis Major, Mars: Implications for the mechanisms of formation, *J. Geophys. Res.*, *110*, E04011, doi:10.1029/2004JE002314.

Barlow, N. G. (2005), A review of Martian impact crater structures and their implications for target properties, in *Large Meteorite Impacts III*, edited by T. Kenkmann, F. Hörz, and A. Deutsch, *Spec. Pap. Geol. Soc. Am.*, *384*, 433–442, doi:10.1130/0-8137-2384-1.433.

Bibring, J.-P., et al. (2006), Global mineralogical and aqueous Mars history derived from OMEGA/Mars Express data, *Science*, *312*(5772), 400–404, doi:10.1126/science.1122659.

Bouley, S., V. Ansan, N. Mangold, P. Masson, and G. Neukum (2009), Fluvial morphology of Naktong Vallis, Mars: A late activity with multiple processes, *Planet. Space Sci.*, *57*(8–9), 982–999, doi:10.1016/j.pss.2009.01.015.

Bouley, S., R. A. Craddock, N. Mangold, and V. Ansan (2010), Characterization of fluvial activity in Parana Valles using different age-dating techniques, *Icarus*, *207*(2), 686–698, doi:10.1016/j.icarus.2009.12.030.

Boyce, J. M., and H. Garbeil (2007), Geometric relationships of pristine Martian complex impact craters, and their implications to Mars geologic history, *Geophys. Res. Lett.*, *34*, L16201, doi:10.1029/2007GL029731.

Carr, M. H. (1996), Channels and valleys on Mars: Cold climate features formed as a result of a thickening cryosphere, *Planet. Space Sci.*, *44*(11), 1411–1423, doi:10.1016/S0032-0633(96)00053-0.

Carr, M. H., and J. W. Head (2010), Geologic history of Mars, *Earth Planet. Sci. Lett.*, *294*(3–4), 185–203, doi:10.1016/j.epsl.2009.06.042.

Chapman, M. G., and K. L. Tanaka (2002), Related magma-ice interactions: Possible origins of chasmata, chaos, and surface materials in Xanthe, Margaritifer, and Meridiani Terrae, Mars, *Icarus*, *155*(2), 324–339, doi:10.1006/icar.2001.6735.

Chassefière, E., F. Leblanc, and B. Langlais (2007), The combined effects of escape and magnetic field histories at Mars, *Planet. Space Sci.*, *55*(3), 343–357, doi:10.1016/j.pss.2006.02.003.

Christensen, P. R., et al. (2003), Morphology and composition of the surface of Mars: Mars Odyssey THEMIS results, *Science*, *300*(5628), 2056–2061, doi:10.1126/science.1080885.

Craddock, R. A., and A. D. Howard (2002), The case for rainfall on a warm, wet early Mars, *J. Geophys. Res.*, *107*(E11), 5111, doi:10.1029/2001JE001505.

Craddock, R. A., and T. A. Maxwell (1990), Resurfacing of the Martian highlands in Amenthes and Tyrrhena region, *J. Geophys. Res.*, *95*, 14,265–14,278, doi:10.1029/JB095iB09p14265.

Craddock, R. A., and T. A. Maxwell (1993), Geomorphic evolution of the Martian highlands through ancient fluvial processes, *J. Geophys. Res.*, *98*, 3453–3468, doi:10.1029/92JE02508.

Craddock, R. A., T. A. Maxwell, and A. D. Howard (1997), Crater morphometry and modification in the Sinus Sabaeus and Margaritifer Sinus regions of Mars, *J. Geophys. Res.*, *102*, 13,321–13,340, doi:10.1029/97JE01084.

Crown, D. A., K. H. Price, and R. Greeley (1992), Geologic evolution of the east rim of the Hellas basin Mars, *Icarus*, *100*(1), 1–25, doi:10.1016/0019-1035(92)90014-X.

Dehouck, E., N. Mangold, S. Le Mouélic, V. Ansan, and F. Poulet (2010), Ismenius Cavus, Mars: A deep paleolake with phyllosilicate deposits, *Planet. Space Sci.*, *58*(6), 941–946, doi:10.1016/j.pss.2010.02.005.

Fassett, C. I., and J. W. Head III (2008), The timing of Martian valley network activity: Constraints from buffered crater counting, *Icarus*, *195*(1), 61–89, doi:10.1016/j.icarus.2007.12.009.

Fassett, C. I., and J. W. Head III (2011), Sequence and timing of conditions on early Mars, *Icarus*, *211*(2), 1204–1214, doi:10.1016/j.icarus.2010.11.014.

Forsberg-Taylor, N. K., A. D. Howard, and R. A. Craddock (2004), Crater degradation in the Martian highlands: Morphometric analysis of the Sinus Sabaeus region and simulation modeling suggest fluvial processes, *J. Geophys. Res.*, *109*, E05002, doi:10.1029/2004JE002242.

Garvin, J. B. (2005), Impact craters on Mars: Natural 3D exploration probes of geological evolution, Abstract 3052 presented at Workshop on The Role of Volatile and Atmospheres on Martian Impact Craters, NASA, Laurel, Md.

Grant, J. A., and S. A. Wilson (2011), Late alluvial fan formation in southern Margaritifer Terra, Mars, *Geophys. Res. Lett.*, *38*, L08201, doi:10.1029/2011GL046844.

Grant, J. A., R. P. Irwin, J. P. Grotzinger, R. E. Milliken, L. L. Tornabene, A. S. McEwen, C. M. Weitz, S. W. Squyres, T. D. Glotch, and B. J. Thomson (2008), HiRISE imaging of impact megabreccia and sub-meter aqueous strata in Holden Crater, Mars, *Geology*, *36*(3), 195–198, doi:10.1130/G24340A.1.

Gulick, V. C., and V. R. Baker (1990), Origin and evolution of valleys on Martian volcanoes, *J. Geophys. Res.*, *95*, 14,325–14,344, doi:10.1029/JB095iB09p14325.

Hartmann, W. K. (2005), Martian Cratering 8: Isochron refinement and the chronology of Mars, *Icarus*, *174*, 294–320, doi:10.1016/j.icarus.2004.11.023.

Hartmann, W. K., and G. Neukum (2001), Cratering chronology and the evolution of Mars, *Space Sci. Rev.*, *96*(1/4), 165–194, doi:10.1023/A:1011945222010.

Hood, L. L., K. P. Harrison, B. Langlais, R. J. Lillis, F. Poulet, and D. A. Williams (2010), Magnetic anomalies near Apollinaris Patera and the Medusae Fossae Formation in Lucus Planum, Mars, *Icarus*, *208*(1), 118–131, doi:10.1016/j.icarus.2010.01.009.

Howard, A. D., and J. M. Moore (2011), Late Hesperian to early Amazonian midlatitude Martian valleys: Evidence from Newton and Gorgonum basins, *J. Geophys. Res.*, *116*, E05003, doi:10.1029/2010JE003782.

Howard, A. D., J. M. Moore, and R. P. Irwin (2005), An intense terminal epoch of widespread fluvial activity on early Mars: 1. Valley network incision and associated deposits, *J. Geophys. Res.*, *110*, E12S14, doi:10.1029/2005JE002459.

Hynek, B. M., R. E. Arvidson, and R. J. Phillips (2002), Geologic setting and origin of Terra Meridiani hematite deposit on Mars, *J. Geophys. Res.*, *107*(E10), 5088, doi:10.1029/2002JE001891.

Irwin, R. P., A. D. Howard, R. A. Craddock, and J. M. Moore (2005), An intense terminal epoch of widespread fluvial activity on early Mars: 2. Increased runoff and paleolake development, *J. Geophys. Res.*, *110*, E12S15, doi:10.1029/2005JE002460.

Ivanov, B. A. (2001), Mars/Moon cratering rate ratio estimates, *Space Sci. Rev.*, *96*(1/4), 87–104, doi:10.1023/A:1011941121102.

Jones, A. P., A. S. McEwen, L. L. Tornabene, V. R. Baker, H. J. Melosh, and D. C. Berman (2011), A geomorphic analysis of Hale crater, Mars: The effects of impact into ice-rich crust, *Icarus*, *211*(1), 259–272, doi:10.1016/j.icarus.2010.10.014.

Kite, E. S., T. I. Michaels, S. Rafkin, M. Manga, and W. E. Dietrich (2011), Localized precipitation and runoff on Mars, *J. Geophys. Res.*, *116*, E07002, doi:10.1029/2010JE003783.

Kraal, E. R., E. Asphaug, J. M. Moore, A. Howard, and A. Bredt (2008), Catalogue of large alluvial fans in Martian impact craters, *Icarus*, *194*(1), 101–110, doi:10.1016/j.icarus.2007.09.028.

Langlais, B., and M. Purucker (2007), A polar magnetic paleopole associated with Apollinaris Patera, Mars, *Planet. Space Sci.*, *55*(3), 270–279, doi:10.1016/j.pss.2006.03.008.

Langlais, B., E. Thébault, and C. Milbury (2011), A magnetic time line for Mars, paper presented at EPSC/DPS meeting, Eur. Planet. Sci. Congr., Nantes, France.

Langlais, B., E. Thébault, Y. Quesnel, and N. Mangold (2012), A Late Martian Dynamo Cessation Time 3.77 Gy Ago, *Proc. Lunar Planet. Sci. Conf.*, *43rd*, 1231.

Levy, J., J. W. Head, and D. R. Marchant (2010), Concentric crater fill in the northern mid-latitudes of Mars: Formation processes and relationships to similar landforms of glacial origin, *Icarus*, *209*(2), 390–404, doi:10.1016/j.icarus.2010.03.036.

Lillis, R. J., M. Manga, D. L. Mitchell, R. P. Lin, and M. H. Acuna (2006), Unusual magnetic signature of the Hadriaca Patera volcano: Implications for early Mars, *Geophys. Res. Lett.*, *33*, L03202, doi:10.1029/2005GL024905.

Lillis, R. J., H. V. Frey, and M. Manga (2008), Rapid decrease in Martian crustal magnetization in the Noachian era: Implications for the dynamo and climate of early Mars, *Geophys. Res. Lett.*, *35*, L14203, doi:10.1029/2008GL034338.

Loizeau, D., et al. (2007), Phyllosilicates in the Mawrth Vallis region of Mars, *J. Geophys. Res.*, *112*, E08S08, doi:10.1029/2006JE002877.

Malin, M. C., and K. S. Edgett (2000), Evidence for recent groundwater seepage and surface runoff on Mars, *Science*, *288*(5475), 2330–2335, doi:10.1126/science.288.5475.2330.

Malin, M. C., and K. S. Edgett (2003), Evidence for persistent flow and aqueous sedimentation on early Mars, *Science*, *302*(5652), 1931–1934, doi:10.1126/science.1090544.

Malin, M. C., et al. (2007), Context Camera Investigation on board the Mars Reconnaissance Orbiter, *J. Geophys. Res.*, *112*, E05S04, doi:10.1029/2006JE002808.

Mangold, N. (2003), Geomorphic analysis of lobate debris aprons on Mars at Mars Orbiter Camera scale: Evidence for ice sublimation initiated by fractures, *J. Geophys. Res.*, *108*(E4), 8021, doi:10.1029/2002JE001885.

Mangold, N. (2011a), Ice sublimation as a geomorphic process: A planetary perspective, *Geomorphology*, *126*(1–2), 1–17, doi:10.1016/j.geomorph.2010.11.009.

Mangold, N. (2011b), Post-early Mars fluvial landforms on mid-latitude impact ejecta, paper presented at 42nd Lunar and Planetary Science Conference, Lunar and Planet. Inst., The Woodlands, Tex.

Mangold, N. (2012), Fluvial landforms on fresh impact ejecta on Mars, *Planet. Space Sci.*, *62*(1), 69–85, doi:10.1016/j.pss.2011.12.009.

Mangold, N., and V. Ansan (2006), Detailed study of an hydrological system of valleys, a delta and lakes in Thaumasia region, Mars, *Icarus*, *180*(1), 75–87, doi:10.1016/j.icarus.2005.08.017.

Mangold, N., C. Quantin, V. Ansan, C. Delacourt, and P. Allemand (2004), Evidence for precipitation on Mars from dendritic valleys in the Valles Marineris Area, *Science*, *305*(5680), 78–81, doi:10.1126/science.1097549.

Mangold, N., et al. (2007), Mineralogy of the Nili Fossae region with OMEGA/Mars Express data: 2. Aqueous alteration of the crust, *J. Geophys. Res.*, *112*, E08S04, doi:10.1029/2006JE002835.

Mangold, N., V. Ansan, P. Masson, C. Quantin, and G. Neukum (2008), Geomorphic study of fluvial landforms on the northern Valles Marineris plateau, Mars, *J. Geophys. Res.*, *113*, E08009, doi:10.1029/2007JE002985.

Mangold, N., J. Carter, F. Poulet, V. Ansan, D. Loizeau, J.-P. Bibring, and S. Murchie (2011), Fluvial landforms and hydrated minerals due to impact craters hydrothermalism on Mars, paper presented at Exploring Mars Habitability, Eur. Space Agency, Lisbon, 13–15 June.

McEwen, A. S., et al. (2007), Mars Reconnaissance Orbiter's High Resolution Imaging Science Experiment (HiRISE), *J. Geophys. Res.*, *112*, E05S02, doi:10.1029/2005JE002605.

McGetchin, T. R., M. Settle, and J. W. Head (1973), Radial thickness variation in impact crater ejecta: Implications for lunar basin deposits, *Earth Planet. Sci. Lett.*, *20*(2), 226–236, doi:10.1016/0012-821X(73)90162-3.

Melosh, H. J. (1989), *Impact Cratering: A Geologic Process, Oxford Monogr. Geol. Geophys.*, vol. 11, Oxford Univ. Press, New York.

Meresse, S., F. Costard, N. Mangold, P. Masson, and G. Neukum (2008), Formation and evolution of the chaotic terrains by subsidence and magmatism: Hydraotes Chaos, Mars, *Icarus*, *194*(2), 487–500, doi:10.1016/j.icarus.2007.10.023.

Mest, S. C., D. A. Crown, and W. Harbert (2010), Watershed modeling in the Tyrrhena Terra region of Mars, *J. Geophys. Res.*, *115*, E09001, doi:10.1029/2009JE003429.

Michael, G. G., and G. Neukum (2010), Planetary surface dating from crater size-frequency distribution measurements: Partial resurfacing events and statistical age uncertainty, *Earth Planet. Sci. Lett.*, *294*(3–4), 223–229, doi:10.1016/j.epsl.2009.12.041.

Milbury, C., and G. Schubert (2010), Search for the global signature of the Martian dynamo, *J. Geophys. Res.*, *115*, E10010, doi:10.1029/2010JE003617.

Milton, D. J., B. C. Barlow, R. Brett, A. R. Brown, A. Y. Glikson, E. A. Manwarin, F. J. Moss, E. C. E. Sedmik, J. Van Son, and G. A. Young (1972), Gosses Bluff impact structure, Australia, *Science*, *175*(4027), 1199–1207, doi:10.1126/science.175.4027.1199.

Moore, J. M., and A. D. Howard (2005), Large alluvial fans on Mars, *J. Geophys. Res.*, *110*, E04005, doi:10.1029/2004JE002352.

Mustard, J. F., B. L. Ehlmann, S. L. Murchie, F. Poulet, N. Mangold, J. W. Head, J.-P. Bibring, and L. H. Roach (2009), Composition, morphology, and stratigraphy of Noachian crust around the Isidis basin, *J. Geophys. Res.*, *114*, E00D12, doi:10.1029/2009JE003349.

Neukum, G., and R. Jaumann (2004), HRSC: The High Resolution Stereo Camera of Mars Express, in *Mars Express: The Scientific Payload*, edited by A. Wilson, pp. 17–35, ESA Publ. Div., Noordwijk, Netherlands.

Papike, J., G. Ryder, and C. Shearer (1998), Lunar samples, in *Planetary Materials, Rev. Mineral. Geochem.*, vol. 36, edited by J. J. Papike, pp. 5,001–5,234, Mineral. Soc. of Am., Chantilly, Va.

Pike, R. J. (1974), Ejecta from large craters on the Moon, *Earth Planet. Sci. Lett.*, *23*(3), 265–271, doi:10.1016/0012-821X(74)90114-9.

Pondrelli, M., A. P. Rossi, L. Marinangeli, E. Hauber, K. Gwinner, A. Baliva, and S. Di Lorenzo (2008), Evolution and depositional environments of the Eberswalde fan delta, Mars, *Icarus*, *197*(2), 429–451, doi:10.1016/j.icarus.2008.05.018.

Poulet, F., J.-P. Bibring, J. F. Mustard, A. Gendrin, N. Mangold, Y. Langevin, R. E. Arvidson, B. Gondet, and C. Gomez (2005), Phyllosilicates on Mars and implications for early Martian climate, *Nature*, *438*(7068), 623–627, doi:10.1038/nature04274.

Quantin, C., P. Allemand, N. Mangold, G. Dromart, and C. Delacourt (2005), Fluvial and lacustrine activity on layered deposits in Melas Chasma, Valles Marineris, Mars, *J. Geophys. Res.*, *110*, E12S19, doi:10.1029/2005JE002440.

Rodriguez, J. A. P., S. Sasaki, R. O. Kuzmin, J. M. Dohm, K. L. Tanaka, H. Miyamoto, K. Kurita, G. Komatsu, A. G. Fairén, and J. C. Ferris (2005), Outflow channel sources, reactivation, and chaos formation, Xanthe Terra, Mars, *Icarus*, *175*(1), 36–57, doi:10.1016/j.icarus.2004.10.025.

Segura, T. L., O. B. Toon, A. Colaprete, and K. Zahnle (2002), Environmental effects of large impacts on Mars, *Science*, *298*(5600), 1977–1980, doi:10.1126/science.1073586.

Segura, T., B. Toon, T. Colaprete, and C. McKay (2007), A sustained greenhouse climate on Mars following an impact event, *Eos Trans. AGU*, *88*(52), Fall Meet. Suppl., Abstract P13B-1292.

Segura, T. L., O. B. Toon, and A. Colaprete (2008), Modeling the environmental effects of moderate-sized impacts on Mars, *J. Geophys. Res.*, *113*, E11007, doi:10.1029/2008JE003147.

Smith, D. E., et al. (1999), The global topography of Mars and implications for surface evolution, *Science*, *284*(5419), 1495–1503, doi:10.1126/science.284.5419.1495.

Squyres, S. W. (1989), Urey prize lecture: Water on Mars, *Icarus*, *79*(2), 229–288, doi:10.1016/0019-1035(89)90078-X.

Toon, O. B., T. Segura, and K. Zahnle (2010), The formation of Martian river valleys by impacts, *Annu. Rev. Earth Planet. Sci.*, *38*, 303–322, doi:10.1146/annurev-earth-040809-152354.

Werner, S. C. (2008), The early Martian evolution—Constraints from basin formation ages, *Icarus*, *195*(1), 45–60, doi:10.1016/j.icarus.2007.12.008.

Werner, S. C., and K. L. Tanaka (2011), Redefinition of the crater-density and absolute-age boundaries for the chronostratigraphic system of Mars, *Icarus*, *215*(2), 603–607, doi:10.1016/j.icarus.2011.07.024.

Wilhelms, D. E. (1973), Comparison of Martian and lunar multiringed circular basins, *J. Geophys. Res.*, *78*, 4084–4095, doi:10.1029/JB078i020p04084.

Wilson, S. A., A. D. Howard, J. M. Moore, and J. A. Grant (2007), Geomorphic and stratigraphic analysis of Crater Terby and layered deposits north of Hellas basin, Mars, *J. Geophys. Res.*, *112*, E08009, doi:10.1029/2006JE002830.

S. Adeli, Planetary Geology, DLR Institute of Planetary Research, Rutherfordstr. 2, D-12489 Berlin, Germany.

V. Ansan, S. Conway, B. Langlais, and N. Mangold, Laboratoire Planétologie et Géodynamique de Nantes, LPGN/CNRS UMR6112 and Université de Nantes, 2 rue de la Houssinière, F-44322 Nantes, France. (nicolas.mangold@univ-nantes.fr)